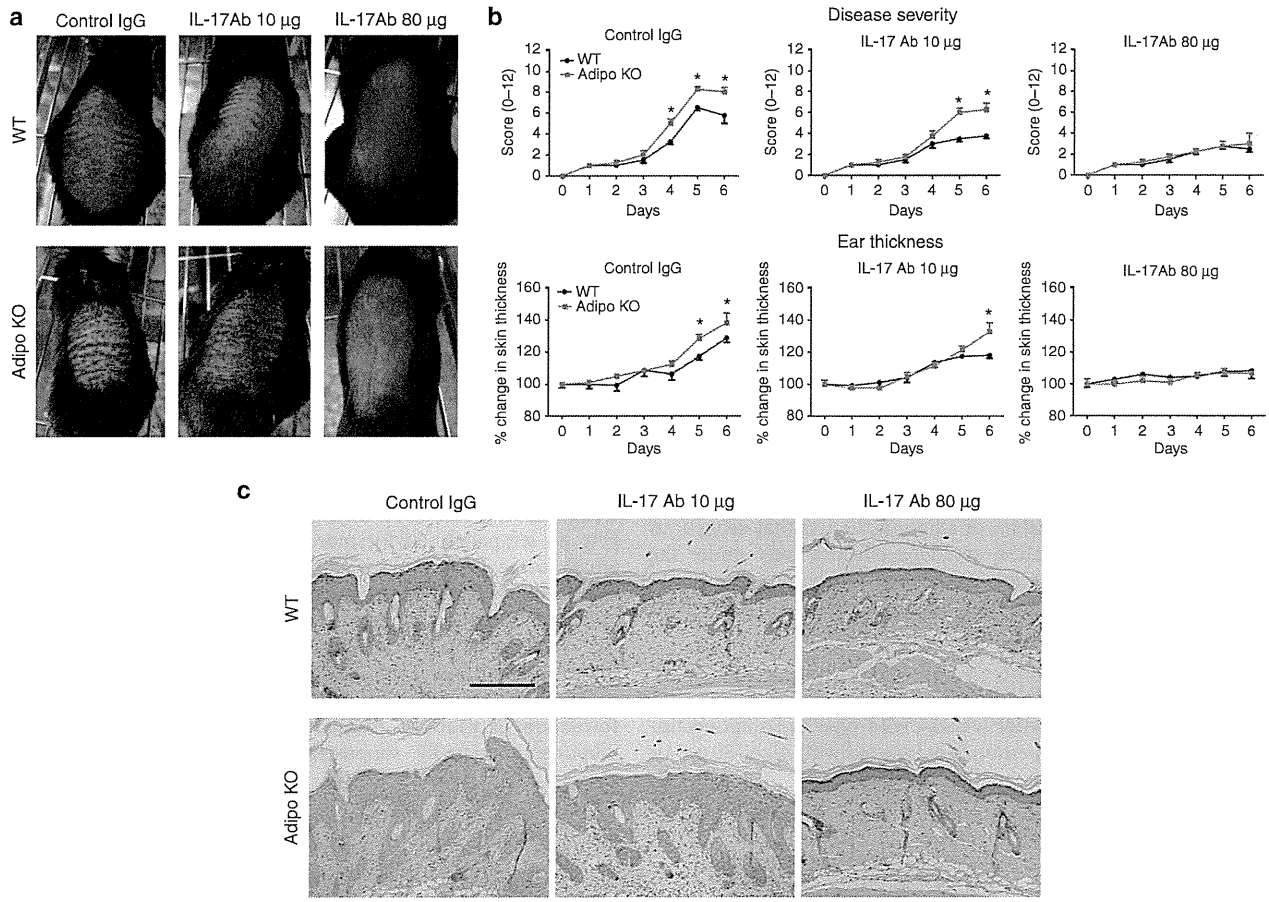

Figure 7 | Adipo knockout (KO) mice need a further dose of anti-IL-17 antibody to prevent the psoriasiform dermatitis. Wild-type (WT) and Adipo KO mice were intraperitoneally injected with control IgG, or 10 and 80 μg of anti-IL-17 antibody (IL-17 Ab) at 1 day before (day −1) and 2 days after (day 2) imiquimod (IMQ) treatment. (**a**) Phenotypical manifestation of WT and Adipo KO mouse back skin induced by IMQ at day 5. (**b**) Disease severity (upper panel) and ear thickness (lower panel) during IMQ treatment. Clinical scores for disease severity were calculated as described in the Methods. Data are presented as mean ± s.e. ($n=4$ for each group). *$P<0.05$ versus WT mice with IMQ application. Data are analysed by Welch's t-test. (**c**) Histological presentation of WT and Adipo KO mouse back skin induced by IMQ at day 5 with the indicated dose of IL-17 antibody injection. Scale bar, 50 μm.

CD4- or CD8-positive T cells. Human CD4- and CD8-positive T cells expressed adiponectin receptor, AdipoR1, but not AdipoR2, at the protein level (Fig. 8c). Peripheral blood mononuclear cells (PBMCs) were activated with IL-23 (0 and 25 ng ml^{-1}), plate-bound anti-CD3 and soluble anti-CD28 with pretreatment of indicated concentrations of adiponectin. IL-17 production by PBMC was inhibited by adiponectin, in a dose-dependent manner up to 25 μg ml^{-1} (Fig. 8d). We also determined the percentage of IL-17-positive cells among CD4- or CD8-positive T cells, activated as mentioned above with or without adiponectin (25 μg ml^{-1}) pretreatment. Flow cytometric analyses revealed the inhibitory effects of adiponectin on human CD4- and CD8-positive T cells (Fig. 8e,f).

Discussion

A number of epidemiologic studies have been focusing on the close relationship between psoriasis and metabolic disorders in terms of adipokines, including adiponectin. However, specific roles of adiponectin in the regulation of skin immune responses remain to be unknown. Using a mouse model of psoriasiform dermatitis, alongside human samples, we set out to determine whether and how adiponectin is involved in the immunological development of psoriasiform skin inflammation in this study. First of all, to confirm that there is not a baseline difference in cutaneous immune responses or epithelia between wild-type and adiponectin-deficient mice, we have conduced contact hypersensitivity experiments on these mice using 2,4-dinitrofluorobenzene or fluorescein isothiocyanate. As shown in Supplementary Fig. 4, no significant difference was observed in mouse ear thickness between these mice in both 2,4-dinitrofluorobenzene- and fluorescein isothiocyanate-applied conditions. We observed that adiponectin deficiency resulted in severe psoriasiform inflammation. Since it is widely known that inhibition of adiponectin upregulates TNF-α production from macrophages or adipocytes[25,43], we expected that the increased skin inflammation in adiponectin-deficient mice was mainly due to the overexpression of TNF-α. Although TNF-α expression was indeed elevated in the inflamed skin of adiponectin-deficient mice, even more striking was the upregulated expression of Th17-related cytokines, IL-17A/IL-17F/IL-22. The regulation of IL-17 by adiponectin was strengthened by the flow cytometric analysis, in which adiponectin deficiency caused increased amount of IL-17 expression by CD3-positive cells on a per-cell basis, along with enhanced recruitment of CD3-positive cells to the skin. In addition, adiponectin exerts a direct suppressive effect on the production of IL-17. Since IL-17 plays central roles in the pathogenesis and maintenance of psoriasis, it could be speculated

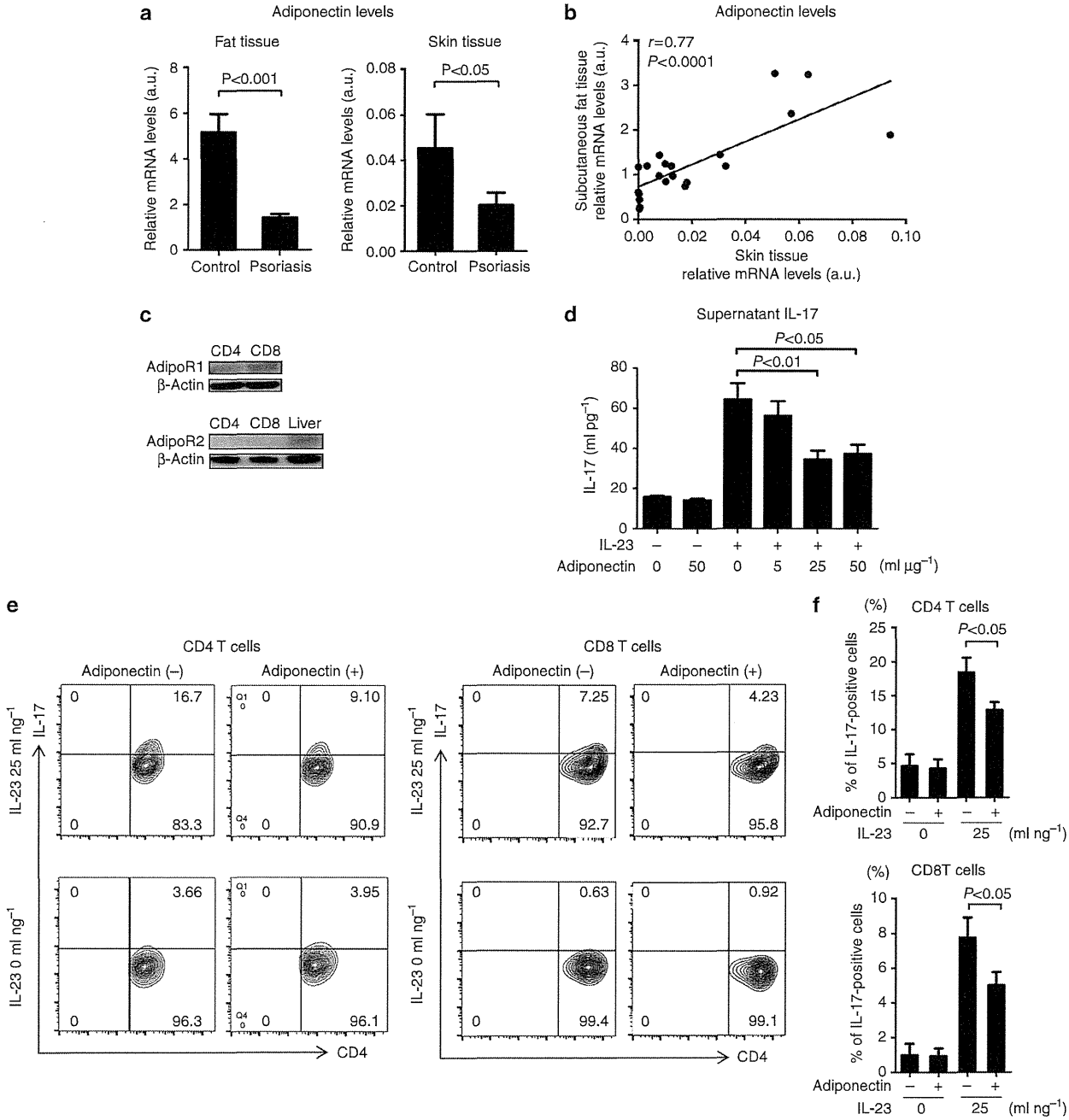

Figure 8 | Adiponectin suppresses IL-17 production from human CD4- and CD8-positive T cells. (**a**) Messenger RNAs of subcutaneous fat (left panel) and skin (middle panel) tissue from psoriasis patients ($n=26$) and healthy controls ($n=12$) were extracted and examined for adiponectin level by quantitative (q)PCR. Data are mean ± s.e. and analysed by Welch's *t*-test. (**b**) Correlation of adiponectin level in psoriasis patients between subcutaneous fat and skin tissue is shown in the right panel. (**c**) Human CD4 and CD8-positive T cells were sorted and were analysed for the expression of adiponectin receptors, AdipoR1 and AdipoR2. (**d**) PBMCs were obtained from human whole blood, and were pretreated with indicated concentrations of adiponectin for 1 h, followed by treatment with plate-bound anti-CD3(5 μg ml^{-1}), soluble anri-CD28 (1 μg ml^{-1}) and IL-23 (0 and 25 ng ml^{-1}) for another 7 days. The supernatant IL-17 levels were determined using the IL-17 ELISA kit. Data are mean ± s.e. ($n=4$) and are representative of two independent experiments. Data are analysed by one-way analysis of variance with Dunnett's multiple comparison test. (**e**) Human PBMCs were treated as mentioned above for 5 days, stimulated with PMA and ionomycin and were stained with antibodies specific for IL-17A as well as CD4 and CD8 cell surface markers, followed by flow cytometric analysis. Data are representative of three independent experiments. (**f**) Graph shows the percentage of IL-17-positive cells among CD4- or CD8-positive T cells ($n=3$: IL-23 0 ng ml^{-1}, $n=6$: IL-23 25 ng ml^{-1}). Data are analysed by Welch's *t*-test.

that adiponectin deficiency would drive skin inflammation, especially IL-17-related psoriasiform inflammation. In the analyses of human samples, psoriasis patients displayed decreased adiponectin levels at both subcutaneous fat and skin site, suggesting that psoriasis patients possess a condition predisposed to produce IL-17 and develop subsequent dermatitis.

Although anti-inflammatory properties of adiponectin have been well-investigated and discussed, most reports have been focusing on the relation between adiponectin and TNF-α or IL-6. Adiponectin suppresses TNF-α or IL-6 production and TNF-α-induced biological effects of certain cells, such as adipocytes, macrophages, endothelial cells and hepatocytes[23,43–45]. These anti-inflammatory and suppressive effects of adiponectin against TNF-α and IL-6 are involved in the pathogenesis of life-related diseases, such as atherosclerosis, insulin resistance or alcoholic/non-alcoholic liver disease, in which these cytokines act as main players in the disease development[46–48]. However, there still exist few reports investigating the function of adiponectin in the regulation of IL-17. Two reports with different disease models have shown the enhanced IL-17 production and disease exacerbation in adiponectin-deficient mice. In the mouse model of multiple sclerosis, which is another representative Th17-related disease, adiponectin-deficient mice developed worse experimental autoimmune encephalomyelitis with higher IL-17 expression of spinal cord tissues[49]. Another report can be obtained from an ozone-induced pulmonary inflammation model, one of the mouse models for asthma, in which adiponectin-deficient mice showed increased ozone-induced inflammation and IL-17A expression in the lung[50]. In the present study, adiponectin-deficient mice developed worse psoriasis inflammation with increased IL-17 expression of the skin, strengthening the hypothesis that adiponectin possesses anti-inflammatory properties in the regulation of IL-17. Another point to be focused on is a time course of IL-6 and IL-17A expression. In the imiquimod-induced skin inflammation, IL-6 expression was first enhanced and thereafter IL-17A expression was upregulated. In addition, IL-6 depletion by IL-6 antibody attenuated about half of IL-17A expression, suggesting that IL-6 might regulate the subsequent IL-17A expression. The function of IL-6 in the differentiation of IL-17A-producing γδ-T cells, which are main producers of IL-17A in the imiquimod-induced dermatitis, is still controversial[51,52]. It has been reported that IL-6-deficient mice showed a twofold decrease in the percentage of IL-17A + cells[51], suggesting a partial contribution of IL-6 in the IL-17A production by γδ-T cells. Thus, it could be speculated that IL-6 overproduction in adiponectin-deficient mice might induce a favourable condition for γδ-T cells to differentiate and produce IL-17A in the development of skin inflammation. In fact, the past report investigating the function of adiponectin in the murine asthma model[50] also demonstrated a similar result to our data, demonstrating upregulated levels of IL-17A in association with IL-6 in lung tissues. Thus, hypoadiponectinemia, associated with IL-6 overproduction, could be responsible for IL-17A development and production.

Chronic inflammation in adipose tissue accelerates obesity-related insulin resistance, leading to the development of the metabolic syndrome, including diabetes mellitus. Increasing evidence from human studies and animal experiments has established TNF-α as a main player of obesity-linked adipose inflammation[18,19]. Recently, besides the classic proinflammatory cytokine TNF-α, the role of IL-17 in adipose tissue and fat metabolism has been drawing attention[53,54]. Clinical studies have demonstrated that obese women exhibit increased levels of circulating IL-23 and IL-17, suggesting a potential role for IL-17 in obesity[55]. As comparable to human studies, several animal experiments indicate that obesity promotes Th17 expansion and subsequent IL-17 production, exacerbating disease severity in murine models of multiple sclerosis and inflammatory bowel disease, both of which are representative Th17-related diseases as well as psoriasis[56]. Furthermore, it has been reported that IL-17A production from PBMCs are increased in type 2 diabetes patients compared with healthy controls[57], and percentage of haemoglobin A1c, a common clinical marker of diabetes severity, is positively correlated with IL-17 production[54]. Thus, IL-17 is now increasingly recognized as a new mediator of adipose tissue metabolism and inflammation, indicating that psoriasis and obesity-related metabolic disorders have a common immunopathological basis in disease development. Although the regulation of IL-17 by adiponectin was revealed by a murine model of psoriasiform dermatitis induced by imiquimod or IL-23, one of the problems in interpreting these data obtained from murine experiments is that chronicity are lacking and different cellular mediators from human psoriasis are involved in this model[34]. A murine model of imiquimod-induced psoriasiform dermatitis is indeed a powerful model to investigate the IL-17-related immunological pathway. However, this model describes an acute and simple skin inflammation, and thus, it has disadvantages in evaluating the maintenance of human chronic disease. Regarding cell types responsible for IL-17 production, γδ-T cells are main producers of IL-17 in a murine model of psoriasiform dermatitis[33,36], whereas γδ-T cells take up a minority of IL-17-producing cells and conventional αβ-T cells produce most of IL-17 in the inflammation site of human psoriasis[58,59]. Thus, we also examined the effect of adiponectin on IL-17 production by human CD4- and CD8-positive T cells. In agreement with the results obtained from the murine experiments, IL-17 production by human CD4- or CD8-positive T cells was dose-dependently suppressed by adiponectin. Since adiponectin level was reduced at the skin, the actual site of inflammation, in psoriasis patients, decreased adiponectin would enhance IL-17 production from CD4- or CD8-positive T cells and finally exacerbate psoriasis dermatitis.

Supplementation of adiponectin ameliorates disease progression induced by adiponectin deficiency in other several murine models[60–62], suggesting that elevation of adiponectin level would be one of the strategies to improve the pathological condition of the disease. Consistent with past reports, exogenous adiponectin supplementation was effective to protect from dermatitis in adiponectin-deficient mice, but interestingly, it was not effective in wild-type mice. One possibility of this discrepancy in responsiveness between wild-type and adiponectin-deficient mice is that the effects of adiponectin might be elicited below a certain concentration and that, above that concentration, the effect might reach a plateau. Thus, it could be speculated that additional administration of exogenous adiponectin to wild-type mice might not have resulted in exerting biological effects. Adiponectin could be used as a potential therapeutic of dermatitis for those with low adiponectin levels, such as diabetic and obese patients, but not for those with sufficient adiponectin levels.

In conclusion, adiponectin plays a crucial role to regulate psoriasis inflammation by directly suppressing IL-17 production from T cells. Our results provide a new therapeutic suggestion that increasing adiponectin levels after diet-induced weight loss would be efficient in improving psoriasis as well as metabolic disorders.

Methods

Mice. Original adiponectin-deficient mice (C57BL/6 and 129/Sv-mixed background)[63] were backcrossed with C57BL/6 mice more than seven times. Mice were 7–10 weeks old for all experiments. Age- and sex-matched wild-type C57BL/6 mice (CLEA Japan, Tokyo, Japan) were used as controls for adiponectin-deficient mice. All mice were maintained under a 12-h light/12 h dark cycle in a specific pathogen-free barrier facility. All studies and procedures were approved by the Committee on Animal Experimentation of Tokyo University.

Induction of psoriasiform skin inflammation by imiquimod. A daily topical dose of 62.5 mg of commercially available imiquimod cream (5%) (Beselna Cream; Mochida Pharmaceuticals, Tokyo, Japan) or control cream (Vaseline and a cream containing isostearic acid) was applied to the shaved back skin and ears of mice for 6 consecutive days (days 0–5). In some experiments, mice were intraperitoneally injected with mouse anti-IL-6 antibody (250 μg per mouse, R&D Systems,

Minneapolis, MN), anti-IL-17 antibody (10 and 70 μg per mouse, R&D Systems) and control rat IgG (R&D Systems). The antibodies were injected 1 day before imiquimod application and day 1 (anti-IL-6 antibody) or day 2 (anti-IL-17 antibody). In the experiments of adiponectin supplementation, mice were given daily intraperitoneal injection of recombinant adiponectin (50 μg per day per mouse)[15] or PBS from 1 day before imiquimod treatment. Disease severity was assessed by using a scoring system based on the clinical Psoriasis Area and Severity Index, except for the affected skin area[32]. To be precise, erythema, scaling and thickening were scored independently on a scale from 0 to 4 (0, none; 1, slight; 2, moderate; 3, marked; 4, very marked), and the cumulative score was used as a total score (scale 0–12).

Induction of psoriasiform skin inflammation by IL-23. Intradermal injections of 10 μl of PBS, either alone or containing 500 ng of recombinant mouse IL-23 (eBioscience, San Diego, CA) were performed into the dorsal aspect of the ear skin. Injections were performed every other day, and skin samples were collected 24 h after the second injection.

Histological and immunohistochemical analyses. Samples of naive or imiquimod-applied mouse back skin were collected. The samples were formalin-fixed and processed for standard haematoxylin and eosin staining. For immunohistochemistry, mouse skin was embedded in optimal cutting compound (OCT), snap-frozen in liquid nitrogen and stored at −80 °C. Cryosections were fixed with cold acetone for 5 min and incubated overnight at 4 °C with anti-mouse major histocompatibility complex class II antibody (1/50 dilution, Abcam, Cambridge, UK) or anti-mouse CD3 antibody (1/100 dilution, Abcam). Tissues were subsequently stained with an avidin–biotin peroxidase complex using a Vector ABC staining kit (Vector Laboratories, Burlingame, CA).

Quantitative real-time reverse transcription-PCR analysis. Total RNA was isolated from mouse back skin using RNeasy fibrous Tissue Mini kits (Qiagen, Germantown, MD) and complementary DNA was synthesized using Superscript III First strand synthesis kits (Invitrogen Life Technologies, Carlsbad, CA). Gene expression was quantified using the TaqMan gene expression assay (Applied Biosystems, Warrington, UK). Primers for TNF-α, IFN-γ, IL-6, IL-12p40, IL-23p19, IL-17A, IL-17F, IL-22 and glyceraldehyde 3-phosphate dehydrogenase (GAPDH) were available from Applied Biosystems. All samples were analysed in parallel for GAPDH gene expression as an internal control. The relative expression levels of each gene were determined by the $2^{-\Delta\Delta^{CT}}$ method.

PCR analysis for the Vγ chain. Epidermal γδ-T cells and dermal γδ-T cells were sorted using FACS Aria II or III. Since a certain population of dermal γδ-T cells is recruited to the epidermis upon imiquimod treatment, epidermal γδ-T cells were collected before imiquimod treatment. Dermal γδ-T cells were collected after imiquimod application. Complementary DNA was synthesized and thermocycled for PCR amplification with 10 μM of each primer and 1.5 U of Taq polymerase (Invitrogen), using the following primers: Vγ4 5′-TGTCCTTGCAACCCCTA CCC-3′, Vg5 5′-TGTGCACTGGTACCAACTGA-3′, Cγ 5′-CTTATGGAGATTT GTTTCAGC-3′, GAPDH 5′-AACTTTGGCATTGTGGAAGG-3′ and 5′-ACACAT TGGGGGTAGGAACA-3′. The nomenclature of TCR Vγ chains is according to Garman[64]. Images have been cropped for presentation. Full-length gel images are shown in Supplementary Fig. 5.

Preparation of cells and flow cytometric analysis. Skin samples applied with imiquimod or control cream for 5 days were incubated in 2 mg ml^{-1} Dispase (Gibco), and were separated into epidermis and dermis. Dermis was minced and then incubated with 2 mg ml^{-1} of collagenase type 2 (Worthington, Lakewood, NJ) in Tyrode buffer for 60–90 min. In some experiments, whole-skin samples were directly minced and digested mentioned above. The digested tissues were centrifuged, resuspended in PBS and filtered through a 70-μm mesh. Single-cell suspensions were stained on ice with either labelled monoclonal antibody or isotype control antibody. Cells were then analysed by FACSVerse flow cytometer (Becton Dickinson, San Jose, CA). The antibodies used were anti-CD3, γδTCR, Vγ4 and Vγ5 (1/100 dilution, Biolegend, San Diego, CA). In selected experiments, intracellular IL-17 staining was performed. Cells were stimulated with plate-bound anti-CD3e monoclonal antibody (BD Pharmingen, San Diego, CA) in the presence of PMA (Sigma, St Louis, MO), ionomycin and brefeldin A (1/1,000 dilution, Biolegend) for 4 h at 37 °C. Cells were first stained with each cell surface antibody and then fixed, permeabilized, followed by anti-mouse IL-17 monoclonal antibody staining (1/100 dilution, Biolegend). Thereafter, the cells were analysed.

Cell sorting. For analysis of *in vitro* experiments, dispase-separated epidermis and dermis were minced and digested as mentioned above, and the cells were sorted on a FACS Aria II or III with a purity of 97–99%.

Immunoblotting. Anti-AdipoR1 and AdipoR2 antibodies were obtained from Immuno-Biological Laboratories (Gunma, Japan). Sorted dermal γδ-T cells and human CD4- and CD8- T cells in lysis buffer were dissolved in NuPAGE LDS Sample Buffer with NuPAGE Sample Reducing Agent (Invitrogen) and denatured by heating for 5 min at 95 °C. Lysis buffer contained 20 mM Tris (pH 7.5), 150 mM NaCl, 1 mM EDTA, 1 mM EGTA, 1% Triton X-100, 2.5 mM sodium pyrophosphate, 1 mM glycerophosphate, 1 mM sodium orthovanadate, 1 mM phenylmethylsulphonyl fluoride and 1 μg ml^{-1} leupeptin. SDS–polyacrylamide gel electrophoresis was performed with NuPAGE 4–12% Bis-Tris gels and MES running buffer (Invitrogen). After transfer to an Immobilon-P transfer membrane (Millipore, Bedford, MA), the membrane was incubated for 1 h at room temperature with blocking buffer, overnight at 4 °C with the primary antibody, anti-AdipoR1 or AdipoR2 antibody (1/25 dilution), washed and incubated for 1 h at room temperature with the appropriate secondary antibody (1/2,000 dilution). After washing, visualization was performed by enhanced chemiluminescent techniques (Thermo Scientific, Rockford, IL). Images have been cropped for presentation. Full-length blotting images are shown in Supplementary Figs 6 and 7.

Secretion of IL-17 from dermal γδ-T cells. Dermal γδ-T cells were sorted as mentioned above. Thereafter, γδ-T cells were cultured with complete medium (RPMI 1640 containing 10% FCS) overnight, and then were incubated with the indicated concentrations of adiponectin for 1 h, followed by treatment with IL-1β (10 ng ml^{-1}; R&D systems) and IL-23 (5 ng ml^{-1}; R&D systems) for another 24 h. The IL-17 protein levels in the supernatants were measured using an ELISA kit from R&D Systems according to the manufacturer's direction.

RNA interference for adiponectin receptors. Accell siRNAs against AdipoR1 and AdipoR2, or nontargeting control siRNA were obtained from Thermo Fischer Scientific (Waltham, MA). All transfections were done using Accell siRNA Reagents following the manufacturer's instructions (Thermo Fischer Scientific). Breifly, isolated γδ-T cells were incubated with Accell siRNA mixed with Accell siRNA delivery medium. After 72 h, transfected γδ-T cells were pretreated with adiponectin (10 μg ml^{-1}) for 1 h, followed by treatment with IL-1β (10 ng ml^{-1}) and IL-23 (5 ng ml^{-1}) for another 6 h. Control experiments have revealed that AdipoR1 and AdipoR2 mRNA levels are reduced by >65%. Gene expression levels of IL-17A were quantified by real-time PCR as described above.

Human subjects. Subcutaneous adipose tissue and skin tissue samples were taken from both psoriasis patients and healthy controls. Samples were taken from 26 patients with psoriasis vulgaris (17 males and 9 females; aged: 51.8 ± 11.9 years) before treatment and 12 healthy controls (8 males and 4 females; aged 49.8 ± 9.4 years). All of the patients were diagnosed with clinical appearance and histological findings. Total RNA was then isolated using Trizol (Invitrogen), after which relative mRNA levels were determined using TaqMan gene expression assay as mentioned above. Institutional approval (University of Tokyo Graduate School of Medicine and Teikyo Universtiy School of Medicine) and written informed consent were obtained from all the subjects. Primers for human adiponectin and GAPDH were available from Applied Biosystems.

Isolation and culture of PBMC. PBMCs were obtained by density centrifugation over Ficoll-Paque (GE Healthcare, Buckinghamshire, UK) and were resuspended in RPMI 1640 supplemented with 10% fetal bovine serum. For IL-17 production, PBMCs were activated by plate-bound anti-CD3 (5 μg ml^{-1}), soluble anti-CD28 (1 μg ml^{-1}) and IL-23 (25 ng ml^{-1}) by pretreatment with indicated concentrations of adiponectin for 1 h. For intracellular staining, PBMCs were incubated for 4 h with PMA and ionomycin in the presence of brefeldin A (all from Sigma) at 37 °C, and intracellular cytokine staining was carried out as mentioned above. The antibodies used were anti-CD4, CD8 and IL-17 (1/100 dilution, all from Biolegend).

Statistical analyses. Data obtained are presented as mean ± s.e. Welch's *t*-test was used for the statistical analysis of differences between two groups. One-way analysis of variance with Dunnett's multiple comparison test was used for statistical analysis of the differences among multiple groups. Values of $P<0.05$ were considered to represent a significant difference.

References

1. Langley, R. G., Krueger, G. G. & Griffiths, C. E. Psoriasis: epidemiology, clinical features, and quality of life. *Ann. Rheum. Dis.* **64,** ii18–ii23 (2005).
2. Myers, W. A., Gottlieb, A. B. & Mease, P. Psoriasis and psoriatic arthritis: clinical features and disease mechanisms. *Clin. Dermatol.* **24,** 438–447 (2006).
3. Lowes, M. A. *et al.* Psoriasis vulgaris lesions contain discrete populations of Th1 and Th17 T cells. *J. Invest. Dermatol.* **128,** 1207–1211 (2008).
4. Di Cesare, A., Di Meglio, P. & Nestle, F. O. The IL-23/Th17 axis in the immunopathogenesis of psoriasis. *J. Invest. Dermatol.* **129,** 1339–1350 (2009).
5. Blauvelt, A. T-helper 17 cells in psoriatic plaques and additional genetic links between IL-23 and psoriasis. *J. Invest. Dermatol.* **128,** 1064–1067 (2008).
6. Chiricozzi, A. & Krueger, J. G. IL-17 targeted therapies for psoriasis. *Expert Opin. Investig. Drugs* **22,** 993–1005 (2013).

7. Kavanaugh, A. *et al.* Ustekinumab, an anti-IL-12/23 p40 monoclonal antibody, inhibits radiographic progression in patients with active psoriatic arthritis: results of an integrated analysis of radiographic data from the phase 3, multicentre, randomised, double-blind, placebo-controlled PSUMMIT-1 and PSUMMIT-2 trials. *Ann. Rheum. Dis.* **73,** 1000–1006 (2014).
8. Tausend, W., Downing, C. & Tyring, S. Systematic review of interleukin-12, interleukin-17, and interleukin-23 pathway inhibitors for the treatment of moderate-to-severe chronic plaque psoriasis: ustekinumab, briakinumab, tildrakizumab, guselkumab, secukinumab, ixekizumab, and brodalumab. *J. Cutan. Med. Surg.* **18,** 1–14 (2014).
9. Davidovici, B. B. *et al.* Psoriasis and systemic inflammatory diseases: potential mechanistic links between skin disease and co-morbid conditions. *J. Invest. Dermatol.* **130,** 1785–1796 (2010).
10. Reich, K. The concept of psoriasis as a systemic inflammation: implications for disease management. *J. Eur. Acad. Dermatol. Venereol.* **26,** 3–11 (2012).
11. Boehncke, W. H., Boehncke, S., Tobin, A. M. & Kirby, B. The 'psoriatic march': a concept of how severe psoriasis may drive cardiovascular comorbidity. *Exp. Dermatol.* **20,** 303–307 (2011).
12. Azfar, R. S. & Gelfand, J. M. Psoriasis and metabolic disease: epidemiology and pathophysiology. *Curr. Opin. Rheumatol.* **20,** 416–422 (2008).
13. Horreau, C. *et al.* Cardiovascular morbidity and mortality in psoriasis and psoriatic arthritis: a systematic literature review. *J. Eur. Acad. Dermatol. Venereol.* **27,** 12–29 (2013).
14. Gulliver, W. Long-term prognosis in patients with psoriasis. *Br. J. Dermatol.* **159,** 2–9 (2008).
15. Boehncke, W. H. & Boehncke, S. Cardiovascular mortality in psoriasis and psoriatic arthritis: epidemiology, pathomechanisms, therapeutic implications, and perspectives. *Curr. Rheumatol. Rep.* **14,** 343–348 (2012).
16. Takahashi, H. & Iizuka, H. Psoriasis and metabolic syndrome. *J. Dermatol.* **39,** 212–218 (2012).
17. Picard, D. *et al.* Increased prevalence of psoriasis in patients with coronary artery disease. Results from a case-control study. *Br. J. Dermatol.* **171,** 580–587 (2014).
18. Osborn, O. & Olefsky, J. M. The cellular and signaling networks linking the immune system and metabolism in disease. *Nat. Med.* **18,** 363–374 (2012).
19. Hotamisligil, G. S. Inflammation and metabolic disorders. *Nature* **444,** 860–867 (2006).
20. Kadowaki, T. *et al.* Adiponectin and adiponectin receptors in insulin resistance, diabetes, and the metabolic syndrome. *J. Clin. Invest.* **116,** 1784–1792 (2006).
21. Diez, J. J. & Iglesias, P. The role of the novel adipocyte-derived hormone adiponectin in human disease. *Eur. J. Endocrinol.* **148,** 293–300 (2003).
22. Ouchi, N. & Walsh, K. Adiponectin as an anti-inflammatory factor. *Clin. Chim. Acta* **380,** 24–30 (2007).
23. Ohashi, K., Ouchi, N. & Matsuzawa, Y. Anti-inflammatory and anti-atherogenic properties of adiponectin. *Biochimie* **94,** 2137–2142 (2012).
24. Fukushima, J. *et al.* Adiponectin prevents progression of steatohepatitis in mice by regulating oxidative stress and Kupffer cell phenotype polarization. *Hepatol. Res.* **39,** 724–738 (2009).
25. Ohashi, K. *et al.* Adiponectin promotes macrophage polarization toward an anti-inflammatory phenotype. *J. Biol. Chem.* **285,** 6153–6160 (2010).
26. Lovren, F. *et al.* Adiponectin primes human monocytes into alternative anti-inflammatory M2 macrophages. *Am. J. Physiol. Heart Circ. Physiol.* **299,** H656–H663 (2010).
27. Takahashi, H. *et al.* Plasma adiponectin and leptin levels in Japanese patients with psoriasis. *Br. J. Dermatol.* **159,** 1207–1208 (2008).
28. Coimbra, S. *et al.* Circulating levels of adiponectin, oxidized LDL and C-reactive protein in Portuguese patients with psoriasis vulgaris, according to body mass index, severity and duration of the disease. *J. Dermatol. Sci.* **55,** 202–204 (2009).
29. Kaur, S., Zilmer, K., Leping, V. & Zilmer, M. The levels of adiponectin and leptin and their relation to other markers of cardiovascular risk in patients with psoriasis. *J. Eur. Acad. Dermatol. Venereol.* **25,** 1328–1333 (2011).
30. Shibata, S. *et al.* Adiponectin as an anti-inflammatory factor in the pathogenesis of psoriasis: induction of elevated serum adiponectin levels following therapy. *Br. J. Dermatol.* **164,** 667–670 (2011).
31. Shibata, S. *et al.* Serum high molecular weight adiponectin levels are decreased in psoriasis patients. *J. Dermatol. Sci.* **55,** 62–63 (2009).
32. van der Fits, L. *et al.* Imiquimod-induced psoriasis-like skin inflammation in mice is mediated via the IL-23/IL-17 axis. *J. Immunol.* **182,** 5836–5845 (2009).
33. Cai, Y. *et al.* Pivotal role of dermal IL-17-producing gammadelta T cells in skin inflammation. *Immunity* **35,** 596–610 (2011).
34. Flutter, B. & Nestle, F. O. TLRs to cytokines: mechanistic insights from the imiquimod mouse model of psoriasis. *Eur. J. Immunol.* **43,** 3138–3146 (2013).
35. Chan, J. R. *et al.* IL-23 stimulates epidermal hyperplasia via TNF and IL-20R2-dependent mechanisms with implications for psoriasis pathogenesis. *J. Exp. Med.* **203,** 2577–2587 (2006).
36. Pantelyushin, S. *et al.* Rorgammat+ innate lymphocytes and gammadelta T cells initiate psoriasiform plaque formation in mice. *J. Clin. Invest.* **122,** 2252–2256 (2012).
37. Gray, E. E. *et al.* Deficiency in IL-17-committed Vgamma4(+) gammadelta T cells in a spontaneous Sox13-mutant CD45.1(+) congenic mouse substrain provides protection from dermatitis. *Nat. Immunol.* **14,** 584–592 (2013).
38. Cai, Y. *et al.* Differential developmental requirement and peripheral regulation for dermal Vgamma4 and Vgamma6T17 cells in health and inflammation. *Nat. Commun.* **5,** 3986 (2014).
39. Yamauchi, T. & Kadowaki, T. Adiponectin receptor as a key player in healthy longevity and obesity-related diseases. *Cell Metab.* **17,** 185–196 (2013).
40. Sutton, C. E. *et al.* Interleukin-1 and IL-23 induce innate IL-17 production from gammadelta T cells, amplifying Th17 responses and autoimmunity. *Immunity* **31,** 331–341 (2009).
41. Palmer, C., Hampartzoumian, T., Lloyd, A. & Zekry, A. A novel role for adiponectin in regulating the immune responses in chronic hepatitis C virus infection. *Hepatology* **48,** 374–384 (2008).
42. Wilk, S. *et al.* Adiponectin is a negative regulator of antigen-activated T cells. *Eur. J. Immunol.* **41,** 2323–2332 (2011).
43. Ajuwon, K. M. & Spurlock, M. E. Adiponectin inhibits LPS-induced NF-kappaB activation and IL-6 production and increases PPARgamma2 expression in adipocytes. *Am. J. Physiol. Regul. Integr. Comp. Physiol.* **288,** R1220–R1225 (2005).
44. Devaraj, S., Torok, N., Dasu, M. R., Samols, D. & Jialal, I. Adiponectin decreases C-reactive protein synthesis and secretion from endothelial cells: evidence for an adipose tissue-vascular loop. *Arterioscler. Thromb. Vasc. Biol.* **28,** 1368–1374 (2008).
45. Zhang, P., Wang, Y., Fan, Y., Tang, Z. & Wang, N. Overexpression of adiponectin receptors potentiates the antiinflammatory action of subeffective dose of globular adiponectin in vascular endothelial cells. *Arterioscler. Thromb. Vasc. Biol.* **29,** 67–74 (2009).
46. Ohashi, K., Shibata, R., Murohara, T. & Ouchi, N. Role of anti-inflammatory adipokines in obesity-related diseases. *Trends Endocrinol. Metab.* **25,** 348–355 (2014).
47. Xu, A. *et al.* The fat-derived hormone adiponectin alleviates alcoholic and nonalcoholic fatty liver diseases in mice. *J. Clin. Invest.* **112,** 91–100 (2003).
48. Luo, N. *et al.* Macrophage adiponectin expression improves insulin sensitivity and protects against inflammation and atherosclerosis. *Diabetes* **59,** 791–799 (2010).
49. Piccio, L. *et al.* Lack of adiponectin leads to increased lymphocyte activation and increased disease severity in a mouse model of multiple sclerosis. *Eur. J. Immunol.* **43,** 2089–2100 (2013).
50. Kasahara, D. I. *et al.* Pulmonary inflammation induced by subacute ozone is augmented in adiponectin-deficient mice: role of IL-17A. *J. Immunol.* **188,** 4558–4567 (2012).
51. Ivanov, I. I. *et al.* The orphan nuclear receptor RORgammat directs the differentiation program of proinflammatory IL-17+ T helper cells. *Cell* **126,** 1121–1133 (2006).
52. Roark, C. L., Simonian, P. L., Fontenot, A. P., Born, W. K. & O'Brien, R. L. gammadelta T cells: an important source of IL-17. *Curr. Opin. Immunol.* **20,** 353–357 (2008).
53. Ahmed, M. & Gaffen, S. L. IL-17 in obesity and adipogenesis. *Cytokine Growth Factor Rev.* **21,** 449–453 (2010).
54. Jagannathan-Bogdan, M. *et al.* Elevated proinflammatory cytokine production by a skewed T cell compartment requires monocytes and promotes inflammation in type 2 diabetes. *J. Immunol.* **186,** 1162–1172 (2011).
55. Sumarac-Dumanovic, M. *et al.* Increased activity of interleukin-23/interleukin-17 proinflammatory axis in obese women. *Int. J. Obes.* **33,** 151–156 (2009).
56. Winer, S. *et al.* Obesity predisposes to Th17 bias. *Eur. J. Immunol.* **39,** 2629–2635 (2009).
57. Zeng, C. *et al.* The imbalance of Th17/Th1/Tregs in patients with type 2 diabetes: relationship with metabolic factors and complications. *J. Mol. Med.* **90,** 175–186 (2012).
58. Nograles, K. E., Davidovici, B. & Krueger, J. G. New insights in the immunologic basis of psoriasis. *Semin. Cutan. Med. Surg.* **29,** 3–9 (2010).
59. Gottlieb, A. B. *et al.* Anti-CD4 monoclonal antibody treatment of moderate to severe psoriasis vulgaris: results of a pilot, multicenter, multiple-dose, placebo-controlled study. *J. Am. Acad. Dermatol.* **43,** 595–604 (2000).
60. Yamauchi, T. *et al.* The fat-derived hormone adiponectin reverses insulin resistance associated with both lipoatrophy and obesity. *Nat. Med.* **7,** 941–946 (2001).
61. Nakatsuji, H., Kishida, K., Sekimoto, R., Funahashi, T. & Shimomura, I. Tracing the movement of adiponectin in a parabiosis model of wild-type and adiponectin-knockout mice. *FEBS Open Bio.* **4,** 276–282 (2014).
62. Shibata, R. *et al.* Adiponectin accumulates in myocardial tissue that has been damaged by ischemia-reperfusion injury via leakage from the vascular compartment. *Cardiovasc. Res.* **74,** 471–479 (2007).
63. Kubota, N. *et al.* Disruption of adiponectin causes insulin resistance and neointimal formation. *J. Biol. Chem.* **277,** 25863–25866 (2002).
64. Raulet, D. H., Garman, R. D., Saito, H. & Tonegawa, S. Developmental regulation of T-cell receptor gene expression. *Nature* **314,** 103–107 (1985).

Acknowledgements

We thank Y. Ito, A and T. Kaga for tissue processing and staining, and C. Ohwashi, T. Ikegami and N. Watanabe for technical assistance. This work was supported by a grant for Research on Intractable Diseases from the Ministry of Health, Labour and Welfare of Japan.

Author contributions

S.S. and Y.T. designed the experiments, analysed the data and wrote the manuscript. S.S. performed most of the experiments' research, with contributions from C.S.Y.H., A.M. and Y.M. All authors discussed the results and commented on the manuscript.

Additional information

Supplementary Information accompanies this paper at http://www.nature.com/naturecommunications

Competing financial interests: The authors declare no competing financial interests.

Reprints and permission information is available online at http://npg.nature.com/reprintsandpermissions/

How to cite this article: Shibata, S. *et al.* Adiponectin regulates psoriasiform skin inflammation by suppressing IL-17 production from γδ-T cells. *Nat. Commun.* 6:7687 doi: 10.1038/ncomms8687 (2015).

ELSEVIER

CrossMark

Experimental Hematology

Experimental Hematology 2015;43:849–857

Targeted gene correction of *RUNX1* in induced pluripotent stem cells derived from familial platelet disorder with propensity to myeloid malignancy restores normal megakaryopoiesis

Hiromitsu Iizuka[a,b], Yuki Kagoya[a,b], Keisuke Kataoka[a,b], Akihide Yoshimi[a,b], Masashi Miyauchi[a,b], Kazuki Taoka[a,b], Keiki Kumano[a,b], Takashi Yamamoto[c], Akitsu Hotta[d,e], Shunya Arai[a,b], and Mineo Kurokawa[a,b]

[a]*Department of Hematology & Oncology, Graduate School of Medicine, University of Tokyo, Tokyo, Japan;* [b]*Core Research for Evolutional Science and Technology (CREST), Japan Science and Technology Agency (JST), Tokyo, Japan;* [c]*Department of Mathematical and Life Sciences, Graduate School of Science, Hiroshima University, Higashi-Hiroshima, Japan;* [d]*Department of Reprogramming Science, Center for iPS cell Research and Applications (CiRA), and Institute for Integrated Cell-Material Sciences (iCeMS), Kyoto University, Kyoto, Japan;* [e]*PRESTO, Japan Science and Technology Agency (JST), Tokyo, Japan*

(Received 4 February 2015; revised 9 May 2015; accepted 10 May 2015)

Familial platelet disorder with propensity to acute myeloid leukemia (FPD/AML) is an autosomal dominant disease associated with a germline mutation in the *RUNX1* gene and is characterized by thrombocytopenia and an increased risk of developing myeloid malignancies. We generated induced pluripotent stem cells (iPSCs) from dermal fibroblasts of a patient with FPD/AML possessing a nonsense mutation R174X in the *RUNX1* gene. Consistent with the clinical characteristics of the disease, FPD iPSC-derived hematopoietic progenitor cells were significantly impaired in undergoing megakaryocytic differentiation and subsequent maturation, as determined by colony-forming cell assay and surface marker analysis. Notably, when we corrected the *RUNX1* mutation using transcription activator-like effector nucleases in conjunction with a donor plasmid containing normal *RUNX1* cDNA sequences, megakaryopoiesis and subsequent maturation were restored in FPD iPSC-derived hematopoietic cells. These findings clearly indicate that the *RUNX1* mutation is robustly associated with thrombocytopenia in patients with FPD/AML, and transcription activator-like effector nuclease-mediated gene correction in iPSCs generated from patient-derived cells could provide a promising clinical application for treatment of the disease.

Familial platelet disorder with propensity to acute myeloid leukemia (FPD/AML) is an autosomal dominant disease characterized by mild to moderate thrombocytopenia, impaired platelet function, and an increased risk for developing hematopoietic malignancies such as myelodysplastic syndrome (MDS) and acute myeloid leukemia [1–3]. The disease is associated with an inherited mutation in the *RUNX1* gene [4], which is located at chromosome 21q22 and known as a transcription factor that regulates fetal and adult hematopoiesis. Genetic mutations and translocations involving *RUNX1* have been reported in a variety of hematopoietic malignancies including MDS and AML [5–8]. Although the prevalence of FPD/AML was initially considered to be very low, there has recently been an increase in the number of reported cases worldwide, along with an increased awareness of FPD/AML by clinicians [9–14]. Because RUNX1 is a key regulator in megakaryocytic differentiation in hematopoiesis [15,16], its mutation is considered to be definitely associated with the pathogenesis of FPD/AML, and developing a gene therapy that corrects the *RUNX1* mutation could lead to fundamental therapeutics for the disease.

Induced pluripotent stem cells (iPSCs) provide an attractive platform for studying heritable diseases [17]. Once iPSCs harboring genomic abnormalities specific for a disease are established, they can be differentiated into cells with relevant lineages. Particularly because sufficient patient samples are not available in rare diseases including FPD/AML, patient-derived iPSCs have great potential as a

Offprint requests to: Mineo Kurokawa, Department of Hematology & Oncology, Graduate School of Medicine, University of Tokyo, 7-3-1 Hongo, Bunkyo-ku, Tokyo 113-8655, Japan; E-mail: kurokawa-tky@umin.ac.jp

0301-472X/
http://dx.doi.org/10.1016/j.exphem.2015.05.004

disease model, as they could generate unlimited quantities of cells. Furthermore, genetic manipulations, such as introduction of exogenous genes and specific correction of the defined mutation in established iPSCs, could lead to novel cellular therapy. Previous studies reported that gene correction of iPSCs from patients with sickle cell anemia, beta thalassemia, and Fanconi anemia successfully reestablished normal hematopoiesis [18–24]. In FPD/AML, *RUNX1*-corrected hematopoietic cells with the capacity to produce both qualitatively and quantitatively normal platelets could be a new source for autologous hematopoietic stem cell transplantation.

In this study, we generated iPSCs from dermal fibroblasts derived from a patient with FPD/AML. Consistent with the clinical phenotype of the disease, we found that FPD iPSC-derived hematopoietic cells had a prominent dysfunction in megakaryocytic differentiation. Additionally, we demonstrated that transcription activator-like effector nuclease (TALEN)-mediated gene correction of the *RUNX1* mutation restored megakaryopoiesis in FPD iPSC-derived hematopoietic cells.

Methods

Generation and culture of iPSCs from a patient with FPD/AML

This research was approved by the ethics committees at the University of Tokyo. Skin biopsy of an adult female patient with FPD/AML was performed after she provided written informed consent. The fibroblasts obtained were culture expanded and reprogrammed to iPSCs as previously described, with retroviral transduction of four factors: *OCT3/4, SOX2, KLF4,* and *c-MYC* [17]. Normal control human iPSCs were established from fibroblasts of healthy volunteers in the same manner. Human iPSCs were routinely maintained on mouse embryonic fibroblast (MEF) feeders and passaged as described previously [25]. Immunofluorescence staining was carried out with Alexa fluor 555 mouse anti-human TRA-1-60 antigen (BD Pharmingen) and Alexa fluor 488 mouse anti-human SSEA4 antigen (BD Pharmingen, San Diego, CA) as described previously [17].

Hematopoietic differentiation of iPSCs

To differentiate iPSCs into hematopoietic cells, we used the same protocol as previously used with embryonic stem cells and iPSCs [26]. In brief, small clusters of iPSCs were transferred onto mitomycin C-treated C3H10T1/2 cells and co-cultured in hematopoietic cell differentiation medium, which consisted of Iscove's modified Dulbecco medium supplemented with a cocktail of 10 μg/mL human insulin, 5.5 μg/mL human transferrin, 5 ng/mL sodium selenite, 2 mmol/L L-glutamine, 0.45 mmol/L monothioglycerol, 50 μg/mL ascorbic acid, and 15% highly filtered fetal bovine serum (FBS) in the presence of 20 ng/mL human vascular endothelial growth factor (VEGF). Culture medium was replaced on days 3, 6, 9, 11, and 13. After 14 to 15 days of culture, the iPSC sacs were crashed with pipette tips and filtered with cell strainer, and $CD34^+CD43^+$ hematopoietic progenitor cells (HPCs) were isolated with anti-CD34 antibody (eBioscience, San Diego, CA) and anti-CD43 antibody (Beckman Coulter, Brea, CA) using FACS Aria II (Becton Dickinson, Franklin Lakes, NJ).

Hematopoietic colony-forming cell assay

Colony-forming cell (CFC) assays for evaluating the capacity to produce erythroid, myeloid, and multilineage cells were performed in MethoCult H4034 semisolid medium (StemCell Technologies). Twenty thousand HPCs harvested from iPSC sacs were plated in 1 mL of medium and cultured for 14 days. Megakaryocytic CFC assays were performed in MegaCult-C semisolid medium (StemCell Technologies). Twenty-five thousand HPCs were cultured in double-chamber slides for 10 to 12 days. Afterward, the slides were dehydrated, fixed, and stained for anti-CD41 antibody according to the manufacturer's protocols. All colonies were classified into three categories: megakaryocytic colony (Mk), mixed Mk colony, and non-Mk colony.

Megakaryocytic differentiation of hematopoietic progenitor cells

To differentiate iPSC-derived HPCs into megakaryocytes, $CD34^+CD43^+$ HPCs were transferred onto mitomycin C-treated C3H10T1/2 cells in six-well plates and maintained in differentiation medium supplemented with 25 mg/mL human megakaryocyte growth and development factor (MGDF), 50 ng/mL human stem cell factor, and heparin. Culture medium was refreshed every 3 days. Nonadherent cells were collected, and CD41a/CD42b positivity was examined with flow cytometry after 9 days of culture [27]. Data analysis was performed with FlowJo software (Treestar, Ashland, OR). The $CD41a^+CD42b^+$ cells were sorted by flow cytometry and stained using the Wright–Giemsa method.

RUNX1 *TALEN construction*

We constructed a pair of TALENs that make DNA double-strand breaks at the site of the *RUNX1* mutation in the REAL assembly method, as previously described [28]. In brief, the plasmids harboring modules of repeat-variable di-residue (RVD) nucleotide, which recognizes each DNA code, were digested with either *Bsa*I or *Bbs*I, and *Bam*HI. The digested strands were ligated in a stepwise manner into designed order. Then the specific DNA sequence recognition parts assembled were inserted into expression vectors, which include the Fok1 nuclease domain. In this way, fusion proteins combining the TALE DNA recognition domain and nuclease domain were made. The donor sequence for homologous recombination was made by using OCT4-2A-EGFP-PGK-puro vector as a backbone vector [29], and *RUNX1* cDNA sequences after the mutation site followed by polyadenylation signal were inserted between approximately 700 bp of homologous arms of both 5′ and 3′ sides.

TALEN-mediated gene correction of iPSCs

We dissociated iPSCs into single cells with Accutase after the Y-27632 treatment and suspended them in Opti-MEM. The TALEN pair and a donor plasmid were transfected with NEPA21 electroporator (Nepa Gene, Ichikawa, Chiba, Japan). After transfection, iPSCs were seeded on MEF feeder cells with supplemented with 10 μmol/L Y-27632. Puromycin was added to iPSC medium 2 days after electroporation, and resistant clones were picked up after 10–14 days. Every puromycin-resistant clone was examined by polymerase chain reaction (PCR) amplification to determine whether insertion accompanied by homologous

recombination has occurred at the specific site. The following primers were used for genomic PCR: primer 1, GAGTCATCAAT TTTATTCTGACTGATCC; primer 2, TAAAGGCAGTGGAGT GGTTCA; primer 3, CCACCAACCTCATTCTGTTT; primer 4, GAGGCGCCGTAGTACAGGT; primer 5, TTTCCAGAACCACA CCCTTC; primer 6, TCCCTCACTCCAAGAAGAGAGTAT. For sequencing of the *RUNX1* cDNA, mutation-containing regions of *RUNX1* were amplified with the following primers: forward, TTTGTCGGTCGAAGTGGAAG; reverse, GGCAATGGATCCC AGGTATT.

Immunoblotting

Total-cell lysates were subjected to immunoblotting. Membranes were probed with anti-RUNX1 (Cell Signaling) and anti-β-actin (Cell Signaling) monoclonal antibody. Detection was performed with horseradish peroxidase-labeled secondary antibodies (Santa Cruz Biotechnology), Immunostar LD Western blotting detection reagent (Wako), and an LAS-3000 image analyzer (FujiFilm).

Real-time quantitative PCR

Real-time quantitative PCR was carried out on the LightCycler480 system (Roche) using SYBR Green reagents according to the manufacturer's instructions. The results were normalized to 18S rRNA levels. Relative expression levels were calculated using the standard curve method. The following primers were used for quantitative PCR experiments: 18S forward, CGCGGTTC TATTTTGTTGGT, and reverse, AGTCGGCATCGTTTATGGTC; *RUNX1* forward, TGGAAGAGGGAAAAGCTTCA, and reverse, TTCTGCCGATGTCTTCGAG.

Results

Generation of iPSCs from a patient with FPD/AML

In this study, we analyzed a patient with FPD/AML of the pedigree we had previously reported [30]. The pedigree displayed a C-T mutation in exon 5 of one of the RUNX1 alleles, changing the codon for the arginine residue at position 174 (runt domain) into a stop codon (R174X mutation). The nonsense mutant has been found to interfere with transactivation by normal RUNX1 in a dominant-negative manner [14]. We established iPSCs from the dermal fibroblasts of the patient by reprogramming with retroviral transduction of *OCT3/4*, *SOX2*, *KLF4*, and *c-MYC*, as previously described [17]. The established FPD iPSCs exhibited characteristic embryonic stem cell-like morphology (Fig. 1A). We also confirmed that they expressed embryonic stem cell gene transcripts, such as *NANOG*, *OCT4*, *REX1*, *SOX2*, and *LIN28* (Fig. 1B), and pluripotent markers SSEA-4 and TRA-1-60, as determined by immunofluorescence staining (Fig. 1C). In addition, the established FPD iPSCs had the same *RUNX1* heterozygous mutation as the patient's primary fibroblasts, indicating that they were truly derived from the patient with FPD/AML (Fig. 1D). Teratoma formation capacity of the iPSCs when they were injected into immunodeficient NOD/scid mice was also confirmed (Fig. 1E).

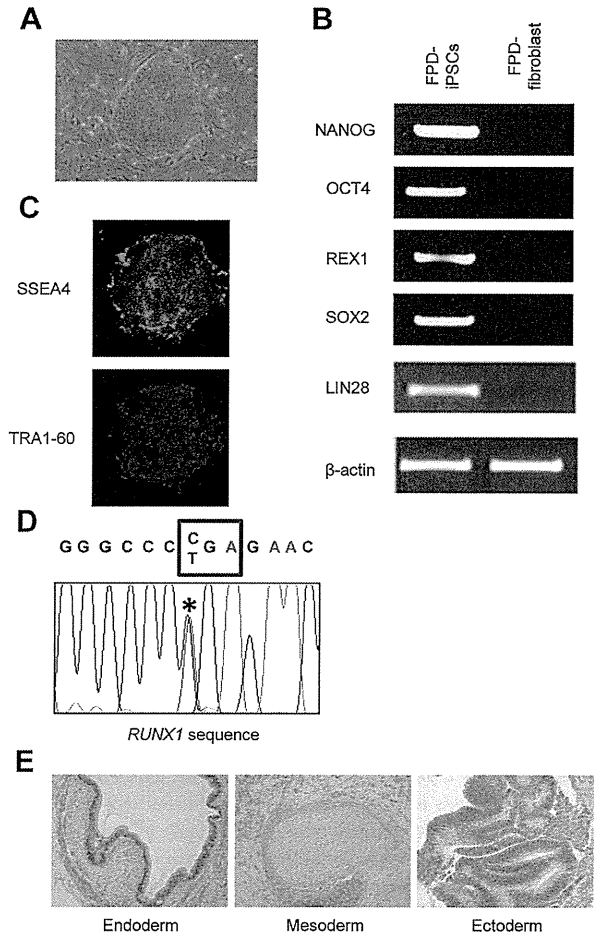

Figure 1. Generation and characterization of induced pluripotent stem cells (iPSCs) from a patient with familial platelet disorder with propensity to acute myeloid leukemia (FPD/AML) (FPD iPSCs). (**A**) Phase contrast micrograph of the morphology of FPD iPSCs. Embryonic stem cell-like colony formation was observed. (**B**) Levels of expression of stem cell genes in FPD iPSCs, compared with those of parental FPD fibroblasts. (**C**) Immunofluorescence staining for pluripotent markers such as SSEA4 and TRA1-60 in FPD iPSCs. (**D**) Genomic sequencing of exon 5 of the *RUNX1* gene in the established FPD iPSCs revealed the same *RUNX1* heterozygous mutation, R174X, as in the patient's primary fibroblasts. * Indicates the point mutation. (**E**) Teratoma formation assay of FPD-derived iPSCs. All three germ layers were included in the tumor. Hematoxylin–eosin stain.

FPD iPSC-derived hematopoietic cells have reduced capacity for megakaryocytic differentiation

To investigate the hematopoietic potential in the established FPD iPSCs, we first differentiated them into HPCs by co-culture with C3H10T1/2 feeder cells. FPD iPSCs yielded $CD34^+CD43^+$ HPCs comparable in frequency to normal iPSCs (Fig. 2A and B). Approximately 10^6 iPSCs generated several hundred thousands of $CD34^+CD43^+$ cells after differentiation culture. Although we tested a prolonged culture period 1 or 2 days longer than usual, HPC yield was not increased (data not shown). Then, the generated $CD34^+CD43^+$ HPCs were seeded into semisolid

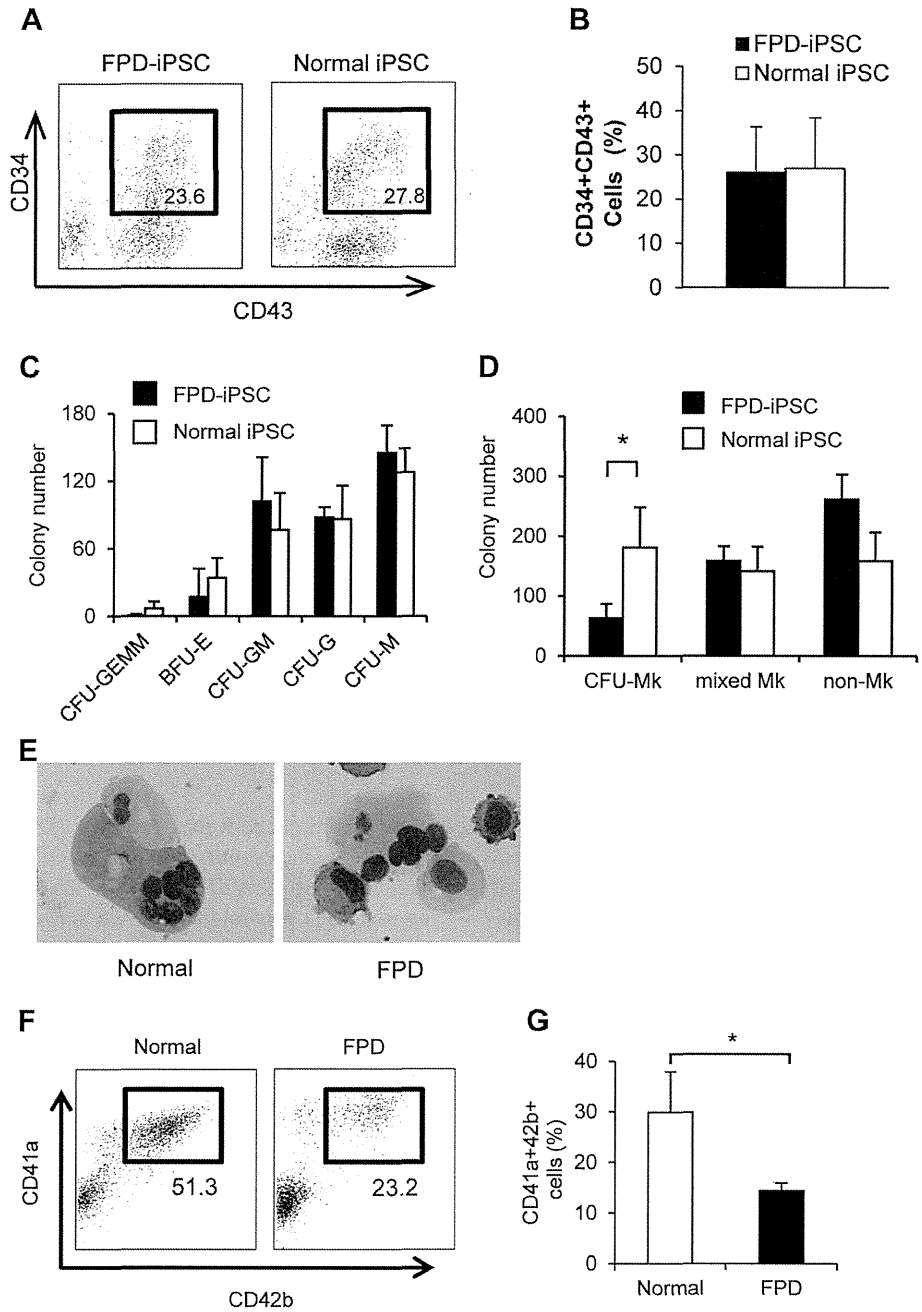

Figure 2. Hematopoietic differentiation capacity of induced pluripotent stem cells (iPSCs) from a patient with familial platelet disorder with propensity to acute myeloid leukemia (FPD/AML) (FPD iPSCs). (**A**, **B**) Flow cytometric analysis of CD34 and CD43 after hematopoietic differentiation of iPSCs: (**A**) representative plots, (**B**) mean percentages of hematopoietic progenitor cells (HPCs0. Experiments were repeated three times independently. Error bars indicate SD. (**C**) Colony-forming cell assay for myeloid and erythroid lineages of HPCs derived from FPD iPSCs and normal counterparts in MethoCult H4034 semisolid medium. (**D**) Colony-forming cell assay for megakaryocytic lineage of HPCs derived from FPD iPSCs, as compared with normal cells, in MegaCult-C semisolid medium. $CD34^{+}CD43^{+}$ cells were sorted and used in the colony-forming assay. Experiments were repeated three times independently. Error bars indicate SD ($*p < 0.05$). (**E**) Wright–Giemsa-stained cytospin images of $CD41a^{+}CD42\ b^{+}$ megakaryocytes differentiated from normal or FPD-derived HPCs. (**F**, **G**) Flow cytometric analysis of CD41a and CD42b after megakaryocytic differentiation of HPCs: (**F**) representative plots, (**G**) mean percentages of $CD41a^{+}CD42b^{+}$ fractions. Experiments were repeated three times independently ($*p < 0.05$). Error bars indicate SD.

culture medium and evaluated for their colony-forming capacity. Notably, while FPD iPSC-derived HPCs exhibited no significant difference in numbers of erythroid and myeloid colonies, compared with the normal control, when seeded into MethoCult H4034 semisolid medium (Fig. 2C), they had a prominently decreased capability for

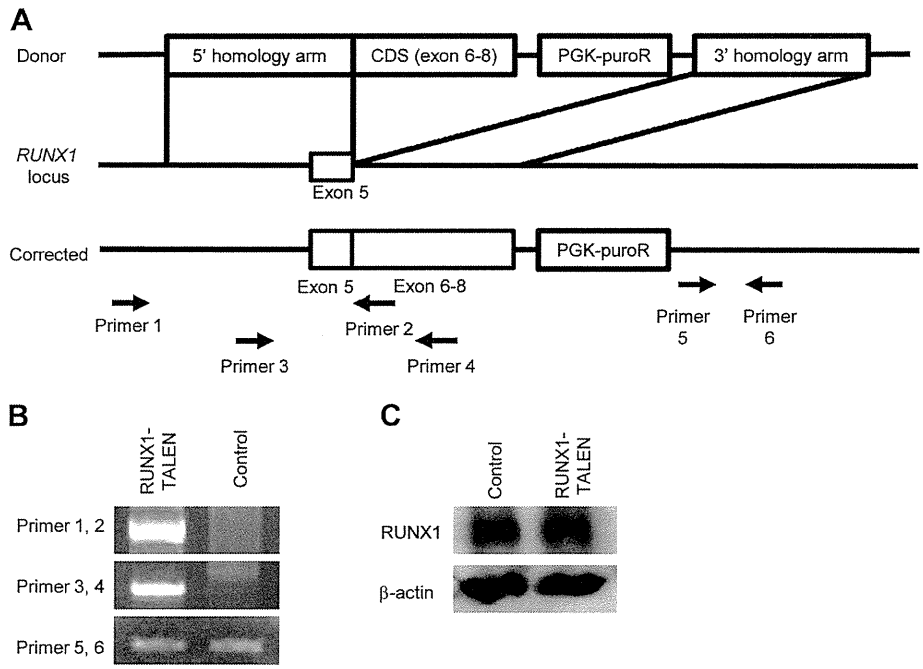

Figure 3. Transcription activator-like effector nuclease (TALEN)-mediated *RUNX1* gene correction. (**A**) Plasmid design for TALEN-mediated correction of *RUNX1* mutation. (**B**) Confirmation of precise integration into HEK293T cells transfected with a pair of TALENs and a donor plasmid with polymerase chain reaction analysis. (**C**) Immunoblot of RUNX1 in HEK293T cells with or without integration of a donor plasmid.

megakaryocytic colony formation as determined by $CD41^+$ CFU-Mk colonies (Fig. 2D). To further evaluate the capacity for differentiation into megakaryocytic lineages of iPSC-derived HPCs, we analyzed the generation and maturation of megakaryocytes after 9 days of culture of HPCs in differentiation medium supplemented with stem cell factor and MGDF on C3H10T1/2 feeder cells. The cytospin image of the $CD41a^+CD42b^+$ cells obtained revealed mature polyploid megakaryocytes in both normal and FPD iPSC-derived cells (Fig. 2E). Interestingly, the differentiation into mature megakaryocytes was less efficient in HPCs derived from FPD iPSCs, as assessed with flow cytometry, than in normal iPSC-derived HPCs, indicating that FPD iPSC-derived HPCs had a reduced capacity for megakaryocyte differentiation and subsequent maturation (Fig. 2F and G).

Design of TALEN plasmids targeting the RUNX1 *mutation site*

Next, we were interested in investigating if repair of the *RUNX1* gene mutation could normalize the capacity for megakaryocytic differentiation in FPD iPSC-derived hematopoietic cells. To specifically correct the *RUNX1* mutation, we used TALENs targeting the region near the mutation site in conjunction with a donor plasmid containing normal *RUNX1* cDNA sequences from exons 6 to 8, as illustrated in Figure 3A. After the pair of TALENs introduces the double-strand break at the target site, homologous recombination between genomic DNA and the donor plasmid replaces mutated *RUNX1* with wild-type cDNA sequences of *RUNX1*. To select the cells with successful homologous recombination, we introduced a puromycin-resistant gene cassette into the donor plasmid. First, we validated the efficacy of our strategy using cell lines. HEK293T cells were transfected with TALEN plasmids and the donor plasmid with electroporation and subsequently cultured for 1 week with 1 μg/mL puromycin, and the genomic DNA of surviving clones was purified. We confirmed that the donor plasmid was precisely integrated at the target site by detecting PCR amplification with the specific primers (Fig. 3B). Also, the protein level of RUNX1 in puromycin-resistant cells was almost the same as that in the control cells, indicating that the inserted *RUNX1* cDNA sequence was properly transcribed and translated into protein (Fig. 3C).

Correction of RUNX1 *mutation in FPD iPSCs restores megakaryopoiesis*

As a next step, we tried to correct the *RUNX1* gene in FPD iPSCs with this strategy. A single-cell suspension of FPD iPSCs was transfected with the two TALEN-encoding plasmids and the donor template, and seeded for colony formation (Fig. 4A). After selection with puromycin, we finally obtained four puromycin-resistant clones, which had proper integration of a donor plasmid as confirmed by genomic PCR analysis. Although only preliminary

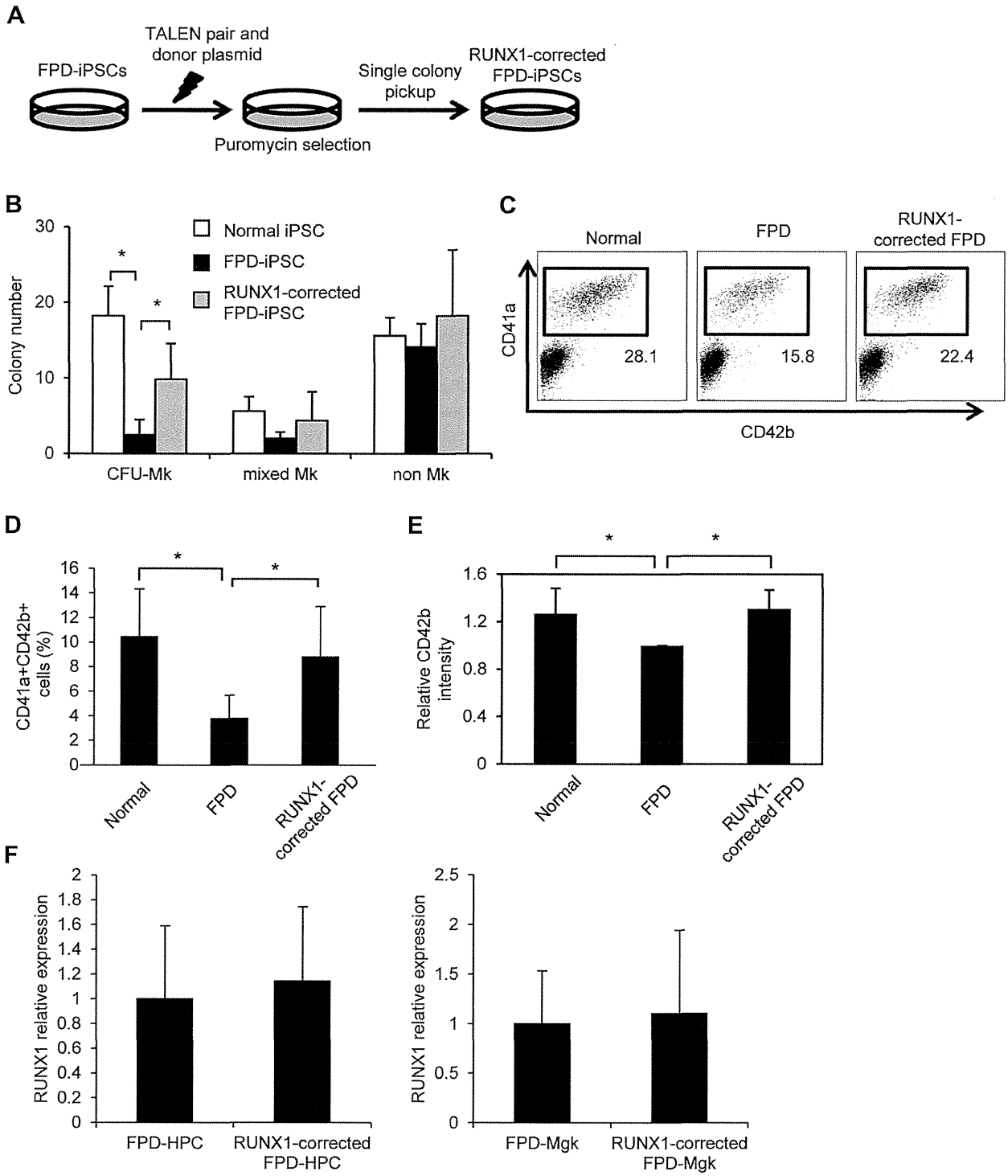

Figure 4. Functional analysis of *RUNX1*-corrected induced pluripotent stem cells (iPSCs) from a patient with familial platelet disorder with propensity to acute myeloid leukemia (FPD/AML) (FPD iPSCs). (**A**) Schematic illustration of generation of transcription activator-like effector nuclease (TALEN)-mediated *RUNX1*-corrected FPD iPSCs. (**B**) Megakaryocytic colony-forming cell assay in MegaCult-C semisolid medium. Experiments were repeated three times independently, and error bars indicate SD (*$p < 0.05$). (**C–E**) Flow cytometric analysis of megakaryocytic differentiation capacity in normal iPSCs, FPD iPSCs, and *RUNX1*-corrected FPD iPSCs: (**C**) representative flow cytometry plots, (**D**) average percentage of $CD41a^+CD42b^+$ cells, and (**E**) and intensity of CD42b expression in three independent experiments. Error bars indicate SD (*$p < 0.05$). (**F**) Relative levels of expression of *RUNX1* in $CD34^+CD43^+$ hematopoietic progenitor cells and $CD41a^+$ megakaryocytes differentiated from *RUNX1*-corrected FPD iPSCs, as compared with those from parental FPD iPSCs. Experiments were repeated three times independently, and the error bars indicate SD.

assessment was performed with three lines of each set of FPD iPSCs and *RUNX1*-corrected iPSCs, they did not seem different in terms of cell biological properties as iPSCs (data not shown). In subsequent analysis, we used one of the *RUNX1*-corrected clones. First, we synthesized a cDNA from mRNA of the clone and confirmed that it possessed a wild-type *RUNX1* sequence without containing a mutant one (data not shown). We differentiated the repaired FPD iPSCs into HPCs and then into megakaryocytes, and evaluated their differentiation efficiency. Consistent with our hypothesis, the HPCs from repaired clones produced significantly increased megakaryocytic colonies (Fig. 4B) and $CD41a^+$ cells compared with the original FPD iPSC-derived HPCs (Fig. 4C and D). Furthermore, they generated more mature megakaryocytes as determined by the intensity of CD42 b within $CD41a^+$ cells (Fig. 4E). Importantly, *RUNX1*-corrected FPD iPSC-derived cells had almost the same levels of *RUNX1* expression as parental FPD iPSC-derived cells throughout the differentiation process (Fig. 4F). These results clearly indicate that TALEN-mediated correction of *RUNX1* gene mutation restores wild-type *RUNX1* expression to physiologic levels and normalizes megakaryopoiesis in hematopoietic cells derived from patients with FPD/AML, which could provide a promising therapeutic approach for fundamental treatment of those patients.

Discussion

In the present study, we generated iPSCs from skin fibroblasts of a patient with FPD/AML. Hematopoietic cells derived from FPD iPSCs exhibited a significantly reduced ability to differentiate into a megakaryocytic lineage compared with the control cells in vitro, which well reflected the clinical features of the disease. In the colony assay, FPD iPSC-derived HPCs exhibited no significant defects in forming erythroid and myeloid colonies. We also found that the megakaryocytes derived from FPD iPSCs had impaired capacity for generating mature megakaryocytes in vitro, indicating that *RUNX1* plays an important role in both differentiation of HPCs into megakaryocytes and their subsequent maturation. These phenotypes were successfully corrected by TALEN-based cleavage at the *RUNX1* mutation site followed by the integration of normal *RUNX1* cDNA sequence. Further technological improvements in TALEN-mediated genome editing are awaited, based on the extremely low efficiency of homologous recombination in our experiments (data not shown).

Gene therapy, which introduces genetic material into cells of patients to manipulate the causative genes, is one of the most promising therapeutic options for inherited disorders. So far, viral vectors have most commonly been used because of their high transduction efficiency compared with nonviral vectors. In hematologic disorders caused by single-gene defects such as several immunodeficiency diseases, autologous transplantation of gene-corrected hematopoietic stem cells is a potentially curative approach and has been the subject of a number of clinical trials [31–36]. One of the most critical concerns regarding the procedure is the risk for insertional mutagenesis, which could trigger oncogenesis as a result of unexpected upregulation of the expression in proto-oncogenes near the vector insertion sites by enhancer sequences within the long-terminal repeat of the retroviral vector, as previously reported [37–41]. Although lentiviral vectors are reported to be safer than retroviral vectors because of the integration sites, as recently reported in the treatment of Wiscott–Aldrich syndrome with autologous transplantation of $CD34^+$ cells lentivirally transduced with the causative gene [42], there still exists a possibility of dismal complications accompanying integration of a transgene [43]. Compared with viral vector-mediated gene addition/complementation, our TALEN-mediated insertion of the desired sequences has several advantages. First, a transgene can be integrated into a highly specific locus by recognition of bilateral homologous arms. Second, because the inserted genes are under the control of physiologic promoter, the repaired clones are expected to fulfill almost normal phenotype, in contrast to the overexpression of wild-type genes by viral vectors, which does not always confer the same phenotypes as those in the endogenous levels of expression. Especially when a causative mutation has a dominant-negative effect as in this case, integration of a normal cDNA sequence at random locations might be insufficient to restore normal function because of the remaining mutant transcripts.

One of the greatest advantages of using iPSCs in gene therapy is that they allow nearly unlimited expansion of hematopoietic cells derived from the patients themselves, which can be used for autologous transplantation after gene correction in vitro. On the other hand, efficient generation of self-renewing long-term hematopoietic stem cells (HSCs) from iPSCs still remains difficult. Previous studies have reported that ESC- or iPSC-derived $CD34^+$ hematopoietic cells could not be efficiently engrafted in the transplanted recipients [44–46]. As maintenance of HSCs requires finely tuned control by bone marrow niches in vivo, it is still challenging to artificially reconstruct the microenvironment in vitro. Although a recent study has reported that engraftable HSCs could be obtained from iPSCs by way of teratoma formation in vivo [47], further studies are required to establish a safe and efficient technology to obtain functional HSCs for future clinical applications. In addition to thrombocytopenia, another critical complication of FPD/AML is its progression to myelogenous leukemia [48]. The increased risk for leukemic transformation might be associated with genomic instability caused by *RUNX1* mutation [49]. Therefore, correction of the mutation is important in preventing the emergence of aberrant clones,

as well as the normalization of platelet counts. Considering the progressive accumulation of DNA damage, it is desirable to repair the mutation as early as possible.

In summary, we generated iPSCs from a patient with FPD/AML and analyzed their characteristics in megakaryocytic differentiation. Dysmegakaryopoiesis associated with *RUNX1* mutation was successfully reverted to normal by TALEN-mediated replacement of mutant *RUNX1* with the wild-type sequence, which could be incorporated into curative therapeutics for thrombocytopenia and prevention of the incidence of myeloid malignancies in patients with FPD/AML.

Acknowledgments

This work was supported by a Grant-in-Aid for Scientific Research from the Japan Society for the Promotion of Science; by Health and Labor Sciences Research grants from the Ministry of Health, Labor and Welfare, Japan (grant number H23-Nanchi-Ippan-104); and by a grant-in-aid from Core Research for Evolutional Science and Technology of Japan (CREST) (grant number 15652256).

The Joung Laboratory REAL Assembly TALEN Kit was kindly provided by JR Yeh via Addgene. The donor plasmid OCT4-2A-EGFP-PGK-puro was kindly provided by R Jaenisch (Addgene plasmid 31938). Human megakaryocyte growth and development factor was generously provided by Kyowa Hakko Kirin Company, Ltd.

Conflict of interest disclosure

The authors have no conflicting financial interests.

References

1. Dowton SB, Beardsley D, Jamison D, Blattner S, Li FP. Studies of a familial platelet disorder. Blood. 1985;65:557–563.
2. Gerrard JM, Israels ED, Bishop AJ, et al. Inherited platelet-storage pool deficiency associated with a high incidence of acute myeloid leukaemia. Br J Haematol. 1991;79:246–255.
3. Arepally G, Rebbeck TR, Song W, Gilliland G, Maris JM, Poncz M. Evidence for genetic homogeneity in a familial platelet disorder with predisposition to acute myelogenous leukemia (FPD/AML). Blood. 1998;92:2600–2602.
4. Song W, Sullivan MG, Legare RD, et al. Haploinsufficiency of CBFA2 causes familial thrombocytopenia with propensity to develop acute myelogenous leukemia. Nat Genet. 1999;23:166–175.
5. Growney JD, Shigematsu H, Li Z, et al. Loss of Runx1 perturbs adult hematopoiesis and is associated with a myeloproliferative phenotype. Blood. 2005;106:494–504.
6. Harada H, Harada Y, Niimi H, Kyo T, Kimura A, Inaba T. High incidence of somatic mutations in the AML1/RUNX1 gene in myelodysplastic syndrome and low blast percentage myeloid leukemia with myelodysplasia. Blood. 2004;103:2316–2324.
7. Kohlmann A, Grossmann V, Klein HU, et al. Next-generation sequencing technology reveals a characteristic pattern of molecular mutations in 72.8% of chronic myelomonocytic leukemia by detecting frequent alterations in TET2, CBL, RAS, and RUNX1. J Clin Oncol. 2010;28:3858–3865.
8. Tang JL, Hou HA, Chen CY, et al. AML1/RUNX1 mutations in 470 adult patients with de novo acute myeloid leukemia: Prognostic implication and interaction with other gene alterations. Blood. 2009; 114:5352–5361.
9. Bujis A, Poddighe P, van Wijk R, et al. A novel CBFA2 single-nucleotide mutation in familial platelet disorder with propensity to develop myeloid malignancies. Blood. 2001;98:2856–2858.
10. Heller PG, Glembotsky AC, Gandhi MJ, et al. Low Mpl receptor expression in a pedigree with familial platelet disorder with predisposition to acute myelogenous leukemia and a novel AML1 mutation. Blood. 2005;105:4664–4670.
11. Sun L, Mao G, Rao AK. Association of CBFA2 mutation with decreased platelet PKC-theta and impaired receptor-mediated activation of GPIIb-IIIa and pleckstrin phosphorylation: Proteins regulated by CBFA2 play a role in GPIIb–IIIa activation. Blood. 2004;103: 948–954.
12. Owen CJ, Toze CL, Koochin A, et al. Five new pedigrees with inherited RUNX1 mutations causing familial platelet disorder with propensity to myeloid malignancy. Blood. 2008;112:4639–4645.
13. Kirito K, Sakoe K, Shinoda D, Takiyama Y, Kaushansky K, Komatsu N. A novel RUNX1 mutation in familial platelet disorder with propensity to develop myeloid malignancies. Haematologica. 2008;93:155–156.
14. Michaud J, Wu F, Osato M, et al. In vitro analysis of known and novel RUNX1/AML1 mutations in dominant familial platelet disorder with predisposition to acute myelogenous leukemia: Implications for mechanisms of pathogenesis. Blood. 2002;99:1364–1372.
15. Elagib KE, Racke FK, Mogass M, Khetawat R, Delehanty LL, Goldfarb AN. RUNX1 and GATA-1 coexpression and cooperation in megakaryocytic differentiation. Blood. 2003;101:4333–4341.
16. Ichikawa M, Asai T, Saito T, et al. AML-1 is required for megakaryocytic maturation and lymphocytic differentiation, but not for maintenance of hematopoietic stem cells in adult hematopoiesis. Nat Med. 2004;10:299–304.
17. Takahashi K, Tanabe K, Ohnuki M, et al. Induction of pluripotent stem cells from adult human fibroblasts by defined factors. Cell. 2007;131: 861–872.
18. Ye L, Chang JC, Lin C, Sun X, Yu J, Kan YW. Induced pluripotent stem cells offer new approach to therapy in thalassemia and sickle cell anemia and option in prenatal diagnosis in genetic diseases. Proc Natl Acad Sci U S A. 2009;106:9826–9830.
19. Wang Y, Jiang Y, Liu S, Sun X, Gao S. Generation of induced pluripotent stem cells from human beta-thalassemia fibroblast cells. Cell Res. 2009;19:1120–1123.
20. Wang Y, Zheng CG, Jiang Y, et al. Genetic correction of beta-thalassemia patient-specific iPS cells and its use in improving hemoglobin production in irradiated SCID mice. Cell Res. 2012;22:637–648.
21. Sebastiano V, Maeder ML, Angstman JF, et al. In situ genetic correction of the sickle cell anemia mutation in human induced pluripotent stem cells using engineered zinc finger nucleases. Stem Cells. 2011; 29:1717–1726.
22. Hanna J, Wernig M, Markoulaki S, et al. Treatment of sickle cell anemia mouse model with iPS cells generated from autologous skin. Science. 2007;318:1920–1923.
23. Ma N, Liao B, Zhang H, et al. Transcription activator-like effector nuclease (TALEN)-mediated gene correction in integration-free β-thalassemia induced pluripotent stem cells. J Biol Chem. 2013;288: 34671–34679.
24. Raya A, Rodriguez-Piza I, Guenechea G, et al. Disease-corrected haematopoietic progenitors from Fanconi anaemia induced pluripotent stem cells. Nature. 2009;460:53–59.
25. Kumano K, Arai S, Hosoi M, et al. Generation of induced pluripotent stem cells from primary chronic myelogenous leukemia patient samples. Blood. 2012;119:6234–6242.
26. Takayama N, Nishikii H, Usui J, et al. Generation of functional platelets from human embryonic stem cells in vitro via ES-sacs, VEGF-promoted structures that concentrate hematopoietic progenitors. Blood. 2008;111:5298–5306.

27. Takayama N, Nishimura S, Nakamura S, et al. Transient activation of c-MYC expression is critical for efficient platelet generation from human induced pluripotent stem cells. J Exp Med. 2010;207:2817–2830.
28. Sander JD, Cade L, Khayter C, et al. Targeted gene disruption in somatic zebrafish cells using engineered TALENs. Nat Biotechnol. 2011;29:697–698.
29. Hockemeyer D, Wang H, Kiani S, et al. Genetic engineering of human pluripotent cells using TALE nucleases. Nat Biotechnol. 2011;29: 731–734.
30. Nishimoto N, Imai Y, Ueda K, et al. T cell acute lymphoblastic leukemia arising from familial platelet disorder. Int J Hematol. 2010;92: 194–197.
31. Aiuti A, Cattaneo F, Galimberti S, et al. Gene therapy for immunodeficiency due to adenosine deaminase deficiency. N Engl J Med. 2009; 360:447–458.
32. Hacein-Bey-Abina S, Hauer J, Lim A, et al. Efficacy of gene therapy for X-linked severe combined immunodeficiency. N Engl J Med. 2010;363:355–364.
33. Boztug K, Schmidt M, Schwarzer A, et al. Stem-cell gene therapy for the Wiskott–Aldrich syndrome. N Engl J Med. 2010;363:1918–1927.
34. Ott MG, Schmidt M, Schwarzwaelder K, et al. Correction of X-linked chronic granulomatous disease by gene therapy, augmented by insertional activation of MDS1-EVI1, PRDM16 or SETBP1. Nat Med. 2006;12:401–409.
35. Candotti F, Shaw KL, Muul L, et al. Gene therapy for adenosine deaminase-deficient severe combined immune deficiency: Clinical comparison of retroviral vectors and treatment plans. Blood. 2012; 120:3635–3646.
36. Nathwani AC, Tuddenham EG, Rangarajan S, et al. Adenovirus-associated virus vector-mediated gene transfer in hemophilia B. N Engl J Med. 2011;365:2357–2365.
37. Hacein-Bey-Abina S, Von Kalle C, Schmidt M, et al. LMO2-associated clonal T cell proliferation in two patients after gene therapy for SCID-X1. Science. 2003;302:415–419.
38. McCormack MP, Rabbitts TH. Activation of the T-cell oncogene LMO2 after gene therapy for X-linked severe combined immunodeficiency. N Engl J Med. 2004;350:913–922.
39. Hacein-Bey-Abina S, Garrigue A, Wang GP, et al. Insertional oncogenesis in 4 patients after retrovirus-mediated gene therapy of SCID-X1. J Clin Invest. 2008;118:3132–3142.
40. Howe SJ, Mansour MR, Schwarzwaelder K, et al. Insertional mutagenesis combined with acquired somatic mutations causes leukemogenesis following gene therapy of SCID-X1 patients. J Clin Invest. 2008;118:3143–3150.
41. Stein S, Ott MG, Schultze-Strasser S, et al. Genomic instability and myelodysplasia with monosomy 7 consequent to EVI1 activation after gene therapy for chronic granulomatous disease. Nat Med. 2010;16: 198–204.
42. Aiuti A, Biasco L, Scaramuzza S, et al. Lentiviral hematopoietic stem cell gene therapy in patients with Wiskott–Aldrich syndrome. Science. 2013;341:1233151.
43. Cesana D, Ranzani M, Volpin M, et al. Uncovering and dissecting the genotoxicity of self-inactivating lentiviral vectors *in vivo*. Mol Ther. 2014;22:774–785.
44. Narayan AD, Chase JL, Lewis RL, et al. Human embryonic stem cell-derived hematopoietic cells are capable of engrafting primary as well as secondary fetal sheep recipients. Blood. 2006;107:2180–2183.
45. Lu M, Kardel MD, O'Connor MD, Eaves CJ. Enhanced generation of hematopoietic cells from human hepatocarcinoma cell-stimulated human embryonic and induced pluripotent stem cells. Exp Hematol. 2009;37:924–936.
46. Ledran MH, Krassowska A, Armstrong L, et al. Efficient hematopoietic differentiation of human embryonic stem cells on stromal cells derived from hematopoietic niches. Cell Stem Cell. 2008;3: 85–98.
47. Amabile G, Welner RS, Nombela-Arrieta C, et al. In vivo generation of transplantable human hematopoietic cells from induced pluripotent stem cells. Blood. 2013;121:1255–1264.
48. Preudhomme C, Renneville A, Bourdon V, et al. High frequency of RUNX1 biallelic alteration in acute myeloid leukemia secondary to familial platelet disorder. Blood. 2009;113:5583–5587.
49. Satoh Y, Matsumura I, Tanaka H, et al. C-terminal mutation of RUNX1 attenuates the DNA-damage repair response in hematopoietic stem cells. Leukemia. 2012;26:303–311.

Article

Cell Reports

Bacterial c-di-GMP Affects Hematopoietic Stem/Progenitors and Their Niches through STING

Graphical Abstract

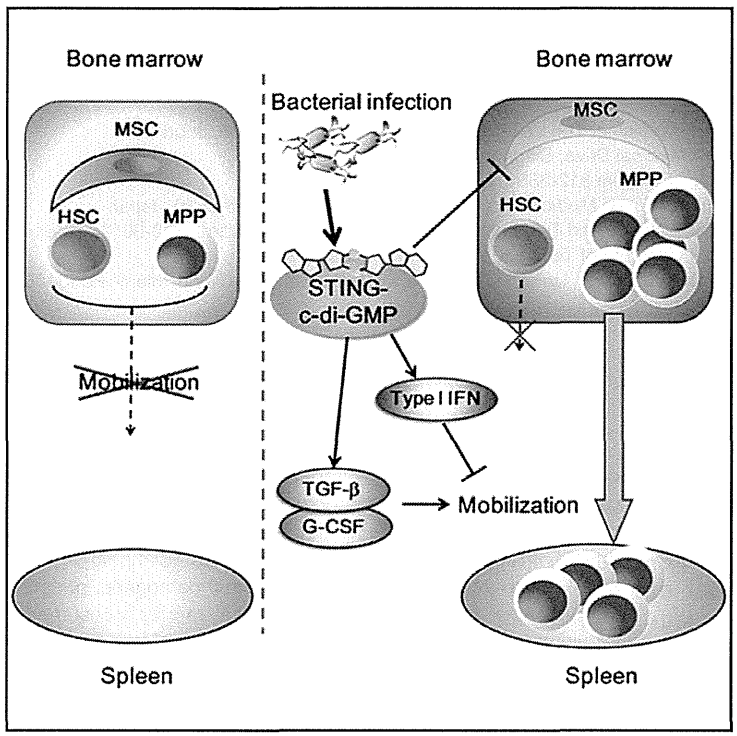

Authors

Hiroshi Kobayashi,
Chiharu I. Kobayashi, ..., Toshio Suda,
Keiyo Takubo

Correspondence

sudato@z3.keio.jp (T.S.),
keiyot@gmail.com (K.T.)

In Brief

Kobayashi et al. report that a bacterial second messenger c-di-GMP influences both HSPCs and their niche cells through STING, thereby inducing expansion and mobilization of multipotent progenitors while decreasing the repopulation capacity of hematopoietic stem cells.

Highlights

- The c-di-GMP/STING pathway attenuates HSC function, and mobilizes HSPCs
- Irf3/IFN activation in HSPCs expands MPP fractions but inhibits HSC mobilization
- TGF-β promotes HSPC mobilization downstream of STING in non-hematopoietic cells

Accession Numbers

GSE65905

Kobayashi et al., 2015, Cell Reports *11*, 71–84
April 7, 2015
http://dx.doi.org/10.1016/j.celrep.2015.02.066

CellPress

Cell Reports
Article

Bacterial c-di-GMP Affects Hematopoietic Stem/Progenitors and Their Niches through STING

Hiroshi Kobayashi,[1,2,3] Chiharu I. Kobayashi,[2] Ayako Nakamura-Ishizu,[2,4] Daiki Karigane,[1,2] Hiroshi Haeno,[5] Kimiyo N. Yamamoto,[5] Taku Sato,[6,7] Toshiaki Ohteki,[6,7] Yoshihiro Hayakawa,[8] Glen N. Barber,[9] Mineo Kurokawa,[3,7] Toshio Suda,[2,4,*] and Keiyo Takubo[1,2,7,*]

[1]Department of Stem Cell Biology, Research Institute, National Center for Global Health and Medicine, Tokyo 162-8655, Japan
[2]Department of Cell Differentiation, The Sakaguchi Laboratory of Developmental Biology, Keio University School of Medicine, Tokyo 160-8582, Japan
[3]Department of Hematology and Oncology, Graduate School of Medicine, The University of Tokyo, Tokyo 113-8655, Japan
[4]Cancer Science Institute, National University of Singapore, 14 Medical Drive, Singapore 117599, Singapore
[5]Department of Biology, Faculty of Sciences, Kyushu University, Fukuoka 812-8581, Japan
[6]Department of Biodefense Research, Medical Research Institute, Tokyo Medical and Dental University, Tokyo 113-8510, Japan
[7]Core Research for Evolutional Science and Technology, Japan Science and Technology Agency, Kawaguchi, Saitama 332-0012, Japan
[8]Department of Applied Chemistry, Faculty of Engineering, Aichi Institute of Technology, Toyota 470-0392, Japan
[9]Department of Cell Biology and the Sylvester Comprehensive Cancer Center, University of Miami Miller School of Medicine, Miami, FL 33136, USA
*Correspondence: sudato@z3.keio.jp (T.S.), keiyot@gmail.com (K.T.)
http://dx.doi.org/10.1016/j.celrep.2015.02.066

SUMMARY

Upon systemic bacterial infection, hematopoietic stem and progenitor cells (HSPCs) migrate to the periphery in order to supply a sufficient number of immune cells. Although pathogen-associated molecular patterns reportedly mediate HSPC activation, how HSPCs detect pathogen invasion in vivo remains elusive. Bacteria use the second messenger bis-(3′-5′)-cyclic dimeric guanosine monophosphate (c-di-GMP) for a variety of activities. Here, we report that c-di-GMP comprehensively regulated both HSPCs and their niche cells through an innate immune sensor, STING, thereby inducing entry into the cell cycle and mobilization of HSPCs while decreasing the number and repopulation capacity of long-term hematopoietic stem cells. Furthermore, we show that type I interferon acted as a downstream target of c-di-GMP to inhibit HSPC expansion in the spleen, while transforming growth factor-β was required for c-di-GMP-dependent splenic HSPC expansion. Our results define machinery underlying the dynamic regulation of HSPCs and their niches during bacterial infection through c-di-GMP/STING signaling.

INTRODUCTION

Hematopoietic stem cells (HSCs) have both self-renewal and multiple differentiation capacities to replenish the entire hematopoietic system throughout the organismal lifespan (Orkin and Zon, 2008). While HSCs remain quiescent in terms of the cell cycle at a steady state, they rapidly re-enter the cell cycle to generate differentiated hematopoietic cells in a demand-driven manner following exposure to various stimuli, including cytotoxic agents, irradiation, and infectious stresses (Blanpain et al., 2011). Upon systemic infection by external pathogens, peripheral immune cells are challenged and rapidly consumed, requiring a continuous supply of leukocytes. Hematopoietic stem and progenitor cells (HSPCs) play a major role in supplying these peripheral immune cells. Various inflammatory cytokines and interferons (IFNs) from immune or infected cells reportedly induce both HSPC cycling and their homing to infectious sites (King and Goodell, 2011). In addition to cytokines, pathogen-associated molecular patterns (PAMPs), including lipopolysaccharide (Nagai et al., 2006), directly stimulate HSPCs through specific pathogen recognition receptors. However, the mechanisms underlying HSPC activity following infectious stress in vivo remain elusive. Bis-(3′-5′)-cyclic dimeric guanosine monophosphate (c-di-GMP) is a second messenger that is utilized ubiquitously by prokaryotes and is associated with numerous bacterial activities, including motility, biofilm formation, and pathogenesis (Hengge, 2009). In addition to its role as a bacterial second messenger, c-di-GMP was recently recognized as an immune-stimulating molecule in mammalian cells (Karaolis et al., 2007). The endoplasmic protein stimulator of IFN genes (STING, also designated TMEM173) was originally identified as an adaptor protein essential for the innate immune response against cytosolic DNA (Ishikawa and Barber, 2008; Zhong et al., 2008). STING is also recognized as an endogenous c-di-GMP receptor, sharing the same signaling pathway with the cytosolic DNA-sensing mechanism (Burdette et al., 2011). Thus, it is essential to determine whether the c-di-GMP/STING pathway functions in host defense mechanisms against bacterial infection and, if so, how that activity affects HSPCs.

In this study, we identify c-di-GMP as a signal-transducing PAMP for HSPCs. We report that c-di-GMP alters HSPC kinetics

and dynamics through the STING pathway, promoting cell cycle entry and expansion of multipotent progenitors (MPPs) as well as mobilization of HSPCs into the spleen. Furthermore, we show that c-di-GMP modulates the bone marrow (BM) microenvironment to induce HSPC mobilization. Overall, we propose that c-di-GMP is a crucial regulator of HSPCs following bacterial infection.

RESULTS

Bacterial Infection Decreases the Number of Long-Term Hematopoietic Stem Cells

To determine how HSPCs respond to septicemia, we used a murine cecal ligation and puncture (CeLP) model to induce poly-microbial intraperitoneal infection (Rittirsch et al., 2009). The number of white blood cells (WBCs) (especially granulocytes) and platelets significantly decreased 48 hr after CeLP, consistent with observations in mice with severe sepsis (Figure 1A). BM cellularity did not significantly decrease (Figure 1B), but, as in peripheral blood (PB), the number of granulocytes decreased while the number of monocytes increased (data not shown). The number of Lin^- $Sca\text{-}1^+$ $c\text{-}Kit^+$ (LSK) cells increased 2-fold, while myeloid progenitors with the marker phenotype Lin^- $c\text{-}Kit^+$ $Sca\text{-}1^-$ (LKS^-) slightly decreased in number (Figure 1C). Although the frequency (Figure 1D) and number (Figure 1E) of MPPs with the phenotypes $CD150^-$ and $CD150^+CD48^+$ LSK expanded 48 hr after CeLP, cells in the highly purified long-term hematopoietic stem cell (LT-HSC) fraction with the marker phenotype $CD150^+CD41^-CD48^-$ LSK (Figure 1E) or $CD150^+CD41^-CD48^-CD34^-Flt3^-$ LSK (Figure 1F) significantly decreased when compared with the sham-surgery group. The CeLP group showed an activated cell-cycle status in each HSPC fraction examined (Figure 1G).

To assess HSPC behavior following infectious stress, we subjected mice to *Salmonella* infection, which induces septicemia, and determined the HSPC number 5 days later (Figure S1A). Similar to CeLP, the number of cells in the LSK fraction, especially MPPs, expanded (Figures S1B–S1D), whereas enriched HSC fractions decreased (Figures S1D and S1E). These findings support the idea that HSPCs directly respond to systemic bacterial infection and that the MPP fraction expands at the expense of the LT-HSC fraction.

c-di-GMP Administration Mimics Bacterial Infection

Toll-like receptor (TLR) signaling and type I IFN signaling are dispensable for HSPC expansion in a CeLP model (Scumpia et al., 2010); therefore, we speculated that other bacteria-specific molecules that circumvent conventional TLR signaling pathways must target HSPCs to stimulate expansion. The c-di-GMP-activated STING/Irf3 axis senses cytosolic DNA independent of TLR signaling (Ishikawa and Barber, 2008; Zhong et al., 2008); therefore, we focused on c-di-GMP as a candidate molecule that could affect HSPC kinetics. To analyze an effect of c-di-GMP on hematopoiesis in vivo, we administered c-di-GMP to mice (Figure 2A). WBC counts, hemoglobin levels, and platelet counts were transiently halved 3 days after c-di-GMP treatment (Figure S2A). The number of bone marrow mononuclear cells (BMMNCs) also decreased (Figure 2B). The frequency of lymphocytes decreased, whereas myeloid cells increased 3 days after c-di-GMP treatment (Figure S2B). However, the number of cells in each differentiated fraction decreased upon c-di-GMP treatment (Figure S2B). Thus, c-di-GMP treatment faithfully mimics the conditions associated with transient pancytopenia observed following severe sepsis, prolonged infection, and immune dysregulation (King and Goodell, 2011).

c-di-GMP Alters HSPC Number and Function in the BM

We next examined the effect of c-di-GMP on immature hematopoietic fractions in the BM. c-di-GMP treatment induced a striking reduction in the number and frequency of all these progenitors in the BM (Figure S2C). c-di-GMP decreased the HSC-enriched fraction in number and frequency (Figures 2C and 2D). Analysis of the LSK fraction revealed that c-di-GMP treatment upregulated Sca-1 expression in a manner similar to that reported following IFN stimulation (Pietras et al., 2014) (Figure 2C), raising the possibility that $Sca\text{-}1^-$ progenitor fractions contaminate the LT-HSC fraction. To minimize this possibility, we examined dye efflux (Challen et al., 2010) (Figures 2E and 2F), activity of an *Evi1*-GFP reporter (which is specifically expressed in the LSK fraction; Kataoka et al., 2011) (Figures 2G and 2H) and CD34 and Flt3 staining (Figures S2D and S2E). The number of $CD150^+CD41^-CD48^-$ LSK *Evi1*$^+$ cells weakly or not stained by Hoechst dye among HSPCs and $CD150^+CD41^-CD48^-CD34^-Flt3^-$ LSK cells decreased (Figures 2F, 2H, and S2E). Overall, the number of HSCs decreased following c-di-GMP treatment.

Furthermore, upon bone marrow transplantation (BMT), c-di-GMP-treated BM cells showed a reduced repopulation capacity (Figure 2I), supporting the idea that the number of functional HSCs decreases following c-di-GMP treatment, as reported for HSPCs in a sepsis model (Burberry et al., 2014). However, HSCs ($CD150^+CD41^-CD48^-CD34^-Flt3^-$ LSK cells) purified following c-di-GMP treatment showed a repopulation capacity comparable to that of control cells, except for at 1 month after BMT (Figure 2J), suggesting that anomalous HSC activity is transient.

By contrast, in c-di-GMP-treated mice, the frequency and number of MPPs, which give rise to all hematopoietic lineages but have a limited self-renewal capacity, exceeded that seen in control mice (Figures 2C and 2D). We also confirmed that the frequency of MPPs, defined as $CD34^+Flt3^+$ LSK cells, increased upon c-di-GMP treatment (Figure S2F). We next examined the effect of c-di-GMP treatment on MPP function, as indicated by short-term reconstitution and in vitro clonogenic capacity. Both $CD150^+CD41/CD48^+$ LSK cells and $CD34^+Flt3^+$ LSK cells from c-di-GMP-treated Ubc-GFP reporter mice, which ubiquitously express GFP, showed reduced short-term reconstitution of myeloid/lymphoid/erythroid/platelet cells (Figure 2K). In addition, colonies derived from single MPPs of c-di-GMP-treated mice were primarily granulocytes and the number of cells per colony was lower than that in controls and was similar to that in the LKS^- fraction. By contrast, STING-deficient cells showed a comparable colony-forming capacity in the presence or absence of c-di-GMP (Figure S2G). This result does not exclude the possibility that LKS^- cells contaminated the LSK fraction. Given that LKS^- cells do not express Flt3, we conclude that

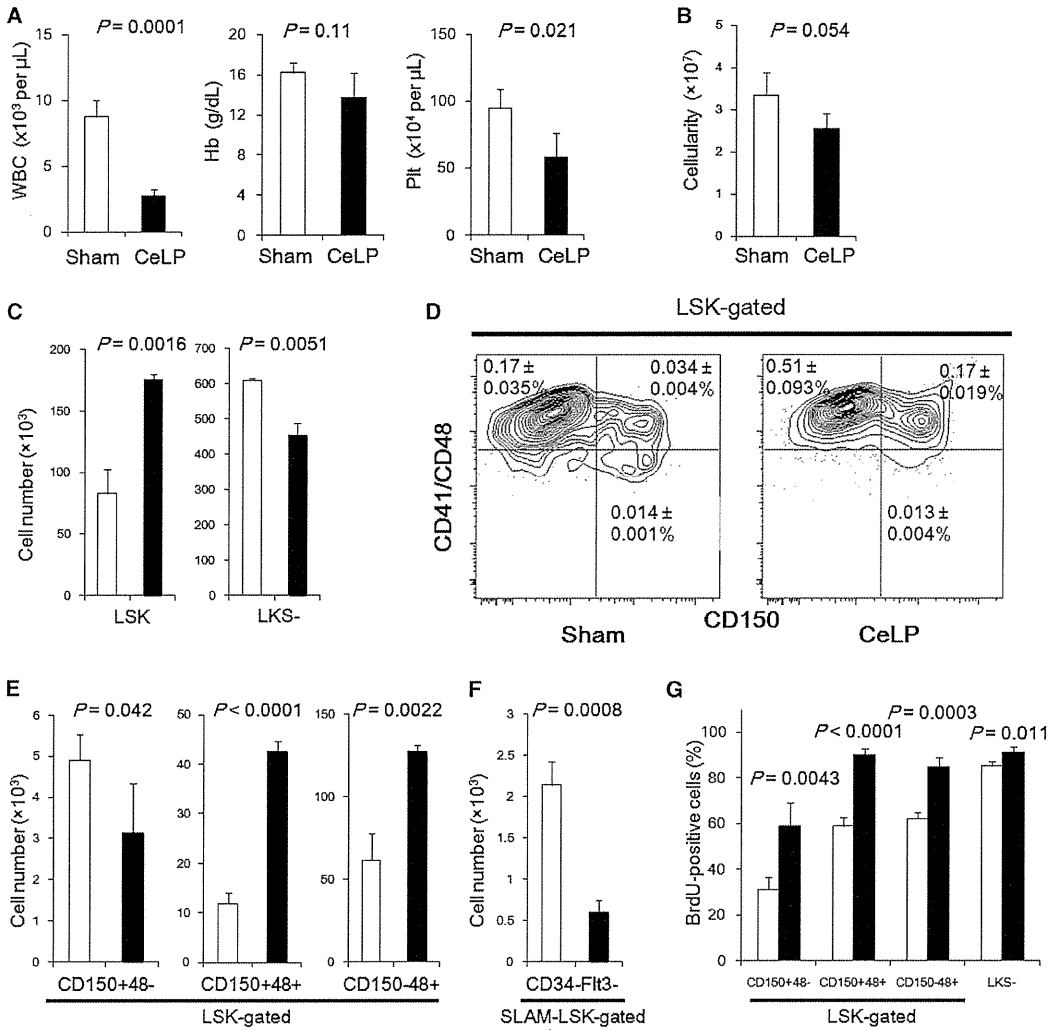

Figure 1. Polybacterial Infection Decreases the Number of LT-HSCs

(A–F) Mice underwent a sham operation (sham, open bars) or CeLP (closed bars) and were sacrificed 48 hr later (mean ± SD, n = 4). (A) Peripheral WBC counts, hemoglobin levels (Hb), and platelet counts (Plt) were examined. (B) Analysis of BM cellularity. (C) The number of LSK cells and myeloid progenitors (LKS^-) from sham (open bars) and CeLP (closed bars) groups (mean ± SD, n = 4). (D) Representative FACS plots of LSK-gated BM cells from sham and CeLP groups. CD150 and CD41/CD48 expression is shown. (E) The number of HSPCs in the LSK fraction from sham (open bars) and CeLP (closed bars) groups (mean ± SD, n = 4). (F) The number of purified HSCs as determined by the marker phenotype $CD150^+CD41^-CD48^-CD34^-Flt3^-$ LSK (mean ± SD, n = 4). SLAM LSK indicates the marker phenotype $CD150^+CD41^-CD48^-$ LSK.

(G) Cell-cycle status was analyzed 48 hr after sham or CeLP surgeries (mean ± SD, n = 3–4). The indicated HSPC fractions in the BM were analyzed by Hoechst 33342 and BrdU staining. The percentages of $BrdU^+$ cells are shown.

See also Figure S1.

following c-di-GMP treatment, the frequency of $CD34^+$ $Flt3^+$ MPP cells increased while their reconstitution potential in BM decreased.

c-di-GMP Dampens the Cell-Cycle Quiescence, Reconstitution Capacity, and Metabolic Status of HSPCs

We next asked how c-di-GMP treatment altered HSC number and function. We assessed the cell-cycle status of HSPCs using short-term bromodeoxyuridine (BrdU) incorporation assays. c-di-GMP induced the proliferation of primitive HSCs, but not of other HSPCs (Figure 2L). Metabolic analysis of HSPCs from c-di-GMP-treated mice revealed reduced intracellular ATP levels and increased lactate dehydrogenase (LDH) activity (Figures S2H and S2I) in $STING^{+/+}$ HSCs and MPPs, which was not seen in $STING^{-/-}$ cells. Several glycolytic genes and tricarboxylic acid (TCA) cycle-associated genes were also inversely regulated in $STING^{+/+}$ cells (Figure S2J). On the other hand, no significant increase in apoptotic cells was detected in the HSPC

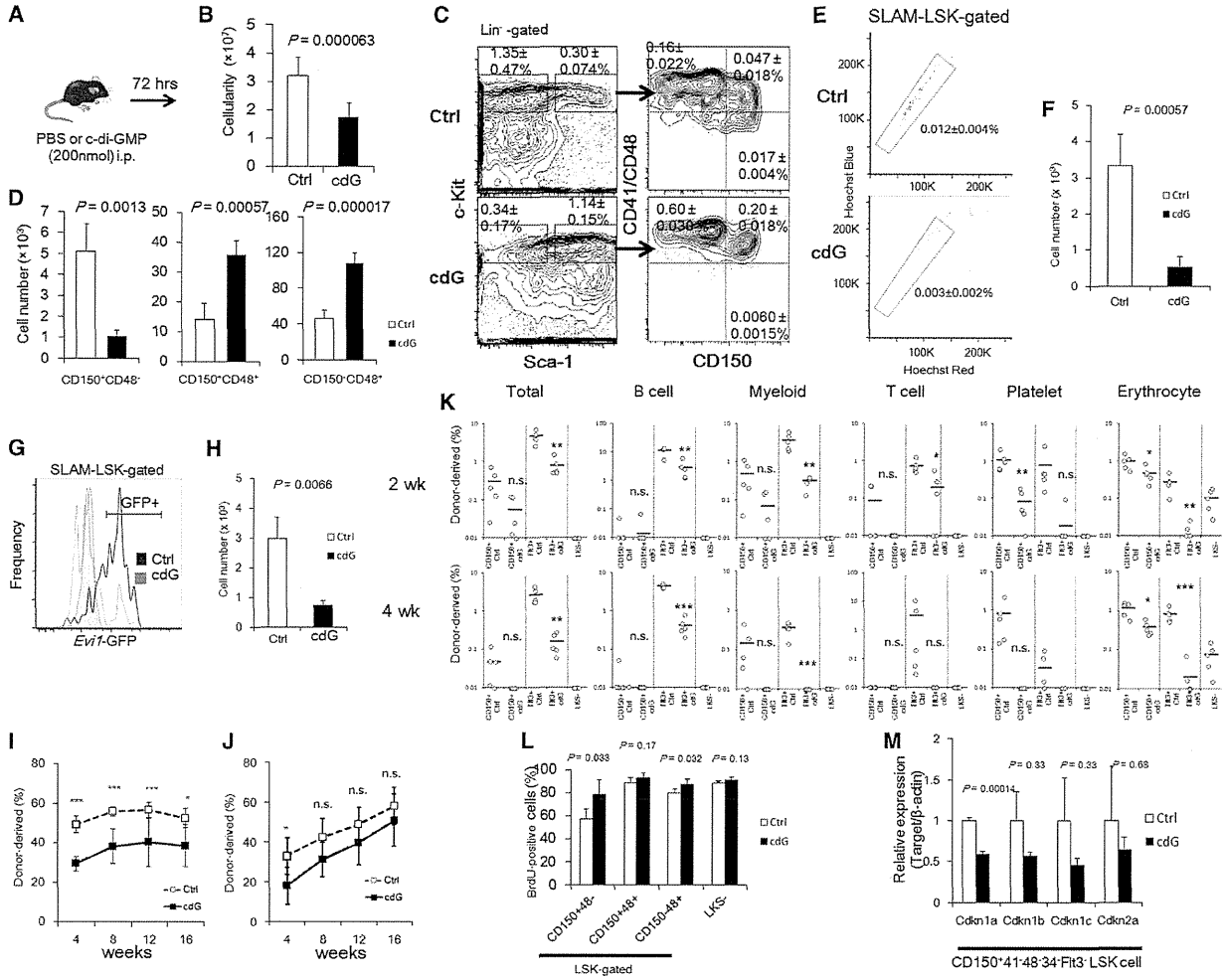

Figure 2. c-di-GMP Administration Induces HSPC Proliferation and Attenuates Their Reconstitution Capacity

(A) Experimental design of in vivo c-di-GMP administration. Mice were intraperitoneally injected with PBS (open bars) or 200 nmol of c-di-GMP (closed bars), and BM cells were analyzed 72 hr later.

(B) The total number of BMMNCs was halved after c-di-GMP treatment (mean ± SD, n = 10 from three independent experiments).

(C) Flow cytometric analysis of the BM HSPC fraction. Representative FACS plots of the Lin$^-$ fraction and the frequency among whole BM cells are shown (mean ± SD, n = 5 from two independent experiments).

(D) The number of cells in the LSK-gated fraction (mean ± SD, n = 5 from two independent experiments). The c-di-GMP-treated group showed a significant decrease in the number of cells in the HSC fraction (CD150$^+$CD41$^-$CD48$^-$LSK), whereas the number of cells in multipotent progenitor fractions (CD150$^+$CD48$^+$ and CD150$^-$CD48$^+$LSK) increased.

(E) Flow cytometric analysis of the BM side population (SP). Representative FACS plots of the CD150$^+$CD41$^-$CD48$^-$ (SLAM) LSK-gated SP fraction and the frequency among whole BM cells are shown (mean ± SD, n = 4).

(F) The number of BM cells residing in the SP among the SLAM LSK-gated fraction (mean ± SD, n = 4).

(G) Gating strategy of *Evi1*$^+$ cells using *Evi1*-GFP reporter mice. A representative histogram of the CD150$^+$CD41$^-$CD48$^-$ (SLAM) LSK-gated fraction is shown. Gray line, *Evi1*$^{+/+}$ mouse; blue line, *Evi1*$^{GFP/+}$ mouse treated with PBS; orange line, *Evi1*$^{GFP/+}$ mouse treated with c-di-GMP.

(H) The number of *Evi1*-GFP$^+$ CD150$^+$CD41$^-$CD48$^-$ LSK cells in the BM from PBS- (Ctlr) or c-di-GMP (cdG)-treated mice (mean ± SD, n = 4 from two independent experiments).

(I) A competitive repopulation assay in which 4 × 10^5 BM cells from mice (Ly5.1) intraperitoneally injected with PBS (Ctrl) or 200 nmol of c-di-GMP (cdG) 3 days before sacrifice were transplanted into lethally irradiated recipients (Ly5.2) together with 4 × 10^5 competitor BM cells (Ly5.2). Percentages of donor-derived cells among PB cells of control (open boxes) or c-di-GMP-treated (closed boxes) mice at the indicated number of weeks after BMT are shown (mean ± SD, n = 6).

(J) A competitive repopulation assay in which 500 sorted LT-HSCs (CD150$^+$CD41$^-$CD48$^-$CD34$^-$Flt3$^-$ LSK) from mice (Ly5.2) intraperitoneally injected with PBS (Ctrl) or 200 nmol of c-di-GMP (cdG) 3 days before sacrifice were transplanted into lethally irradiated recipients (Ly5.1) together with 4 × 10^5 competitor BM cells (Ly5.1). Percentages of donor-derived cells among PB cells of control (open boxes) or c-di-GMP-treated (closed boxes) groups at the indicated number of weeks after BMT are shown (mean ± SD, n = 6; representative of three independent experiments).

(legend continued on next page)